FIELD AND MODELING INVESTIGATIONS INTO THE DRIVERS AND IMPLICATIONS OF BEACH AND SALTMARSH SHORELINE EROSION: EXAMINING THE IMPACTS OF GEOMORPHIC CHANGE ON COASTAL CARBON BUDGETS AND THE ROLE OF SEA-LEVEL ANOMALIES IN FACILITATING BEACH EROSION

Ethan John Theuerkauf

A dissertation submitted to the faculty at the University of North Carolina at Chapel Hill in partial fulfillment of the requirements for the degree of Doctor of Philosophy in the Department of Marine Sciences in the College of Arts and Sciences.

Chapel Hill
2016

Approved by:

Antonio B. Rodriguez

Carolyn A. Currin

Stephen R. Fegley

Richard A. Luettich, Jr.

Brent A. McKee

ABSTRACT

Ethan John Theuerkauf: Field and modeling investigations into the drivers and implications of beach and saltmarsh shoreline erosion: Examining the impacts of geomorphic change on coastal carbon budgets and the role of sea-level anomalies in facilitating beach erosion.
(Under the direction of Antonio B. Rodriguez)

Coastal landscapes, such as saltmarshes and barrier islands, evolve across timescales ranging from storm events to millennia in response to a number of physical and anthropogenic drivers. Proper management of these dynamic environments hinges upon a strong scientific understanding of the processes that shape the coast as well as the implications of coastal change. The first chapter of this dissertation presents measurements of beach erosion along a transgressive barrier island related to sea-level anomalies, which are short-term, non-storm fluctuations in water level. These phenomena are recognized along entire continental margins, but are not included in coastal management plans. Erosion measurements from a barrier island in North Carolina indicated that similar amounts of erosion were observed in a year with frequent sea-level anomalies as a year with a hurricane impact. This work suggests that anomalies can exacerbate the impacts of storms, long-term sea-level rise, and human impacts. The second chapter describes a carbon budget model that was developed for mainland fringing saltmarshes that includes shoreline erosion, which is a process largely ignored in marsh carbon assessments. The final chapter extends the marsh carbon budget to transgressive barrier islands and explores the impact of erosion, overwash, and geologic setting on barrier island carbon budgets and reservoirs. Saltmarshes are considered carbon sinks because of high carbon burial rates and a carbon reservoir that is presumed to increase through time; however, the global

prevalence of marsh loss suggests that marsh carbon budgets must also include carbon export from erosion. Carbon budget box models for mainland fringing saltmarshes and transgressive barrier islands were developed that include both carbon storage across the marsh platform and carbon export from shoreline erosion. The fringing marsh model was applied at an eroding fringing marsh and the output indicates that erosion can switch a marsh from functioning as a sink to a source. The barrier island model was applied at two transgressive barriers and results suggest that erosion, overwash, and human impacts contribute to the transition of a barrier to a carbon source, which results in a reduction in the carbon reservoir through time.

To my wife and best friend Kristen Theuerkauf. Thank you for the sacrifices and support throughout this journey.

ACKNOWLEDGEMENTS

I extend my utmost appreciation and gratitude to my advisor Tony Rodriguez. It has been an honor to learn from you as your student over the past 7 years and I am excited for our future as colleagues and friends. I owe so much of the wonderful experience I had at UNC to the time shared with you. Whether it was road trips to conferences or field work, animated discussions about data, or breakfasts at the Captain's Table it always a blast. Thank you for taking me under your wing and not only teaching me how to be a coastal geologist, but also for treating me like part of your family. The unwavering support of my wife Kristen has been the driving force in my scientific career. She has encouraged me through all my endeavors and has inspired me to want to strive for greatness. Thank you for standing by my side through it all. My time in graduate school afforded me the opportunity to make friendships that I will cherish for life. Particularly my good friend, colleague, and SciREN co-founder Justin Ridge. You taught me how to be a good friend and a good person and for that I am forever grateful. I know that great memories are in store for us in the future. I appreciate all of the feedback, support, and guidance that my committee, Carolyn Currin, Steve Fegley, Brent McKee, and Rick Luettich, has provided me over the years. It has been a pleasure to work with you all. Lastly, I want to thank the Institute of Marine Sciences and Department of Marine Sciences community. I especially want to thank Michelle Brodeur and Beth VanDusen for their friendship and Kerry Irish for bringing out the science communicator in me.

TABLE OF CONTENTS

LIST OF TABLES

LIST OF FIGURES

LIST OF ABBREVIATIONS AND SYMBOLS

AWAC	Acoustic Wave and Current Profiler
AD	Anno Domini
ANOVA	Analysis of Variance
AMOC	Atlantic Meriodional Overturning Circulation
BP	Before Present
C	carbon
cm	centimeter
CO_2	carbon dioxide
R^2	coefficient of determination
DSAS	Digital Shoreline Analysis System
ENSO	El Niño-Southern Oscillation
g	grams
ICW	Intracoastal Waterway
i.e.	that is
km	kilometer
NAVD88	North American Vertical Datum of 1988
NAO	North Atlantic Oscillation
m	meter
MDOE	Maximum Depth of Erosion
MSL	mean sea level
mm	millimeter
N	North

NOAA	National Oceanic and Atmospheric Administration
NC	North Carolina
NCDCM	North Carolina Division of Coastal Management
NDBC	National Data Buoy Center
Pg	petagram
RTK-GPS	Real Time Kinematic Global Positioning System
s	seconds
SD	standard deviation
Hs	significant wave height
U.S.	United States
USA	United States of America
USDA	United States Department of Agriculture
W	West
yr	year
~	around

CHAPTER 1: SEA LEVEL ANOMALIES EXACERBATE BEACH EROSION[1]

1. Introduction

The morphologic responses of beaches to sea level rise over short (storm surge) and long (eustatic sea level change) time frames are well documented and generally include erosion, overwash and breaching during storms, and landward translation of the shoreline as ocean volume increases over centuries to millennia (e.g., Zhang et al., 2004; Rodriguez and Meyer, 2006; Culver et al., 2007; Stockdon et al., 2007; Timmons et al., 2010). In addition, climate cycles such as El Niño-Southern Oscillation (ENSO) and the North Atlantic Oscillation (NAO) that operate at seasonal to multi-year time scales produce sea level highs that have been documented to enhance the magnitude of erosion and morphologic changes to beaches when they coincide with large storms (Storlazzi and Griggs, 2000; Ruggiero et al., 2001; Dingler and Reiss, 2002; Keim et al., 2004; Allan and Komar, 2006; Eichler and Higgins, 2006; Vespremeanu-Stroe et al., 2007). Unlike sea level highs from climate cycles, intra-seasonal sea level changes (weeks to months), such as an increase in sea level along the U.S. East Coast resulting from a decrease in the strength of the Gulf Stream, do not always coincide with large storms (Blaha, 1984; Ezer, 2001; Ezer et al., 2013). Those intra-seasonal highs, or coastal sea level anomalies, may influence beach morphology; however, assessments of their impacts are lacking. As a result, sea level anomalies are currently ignored in parameterizing shoreline-response models and beach management plans.

[1] 1 This chapter previously appeared as an article in Geophysical Research Letters. The original citation is as follows: Theuerkauf, E.J., Rodriguez, A.B., Fegley, S.R., and Luettich, R.A. Jr., 2014. Sea-level anomalies exacerbate beach erosion, Geophys. Res. Lett., 41(14), 5139-5147.

Coastal sea level anomalies arise from meteorological and oceanographic forcing mechanisms and have been observed globally (Kolker and Hameed, 2007) but may be more prominent and spatially uneven along the U.S. East Coast due to the influence of the Atlantic Meriodional Overturning Circulation (AMOC) and the Gulf Stream (Sweet et al., 2009; Sallenger et al., 2012; Ezer, 2013; Ezer et al., 2013). Sea level anomalies impact coastal areas by changing the hydro-period of intertidal habitats (Morris et al., 1990) and result in beach morphologic change by shifting the zone of wave influence landward. Anomalies add to the erosive forces of storms and accelerated relative sea level rise (Sweet and Zervas, 2011). Here, we explore morphologic changes to a barrier-island beach experiencing several sea level anomalies in a year. The objective is to compare the relative effectiveness of beach erosion due to typical wave conditions during sea level anomalies with that due to more extreme waves generated by Hurricane Irene during a time of non-anomalous sea level.

2. Study Area

Onslow Beach, North Carolina, USA, is a wave-dominated barrier island, located in Onslow Bay between Cape Fear and Cape Lookout (Figure 1.1). The island has a sinusoidal shape with a central headland flanked by embayments on either end of the island (Figure 1). Beach gradients are steeper along the headland than the adjacent embayments (Rodriguez et al., 2012). The southwestern part of the barrier has a typical transgressive morphology, including narrow and discontinuous low-elevation dunes, multiple washover fans, a narrow beach, and a shoreline that has been moving consistently landward over decadal time scales. The morphology of the northeastern part of the island is typical of an aggradational barrier, with continuous high-elevation dunes, a wide beach, and a shoreline that has been relatively stationary over decadal

Figure 1.1:

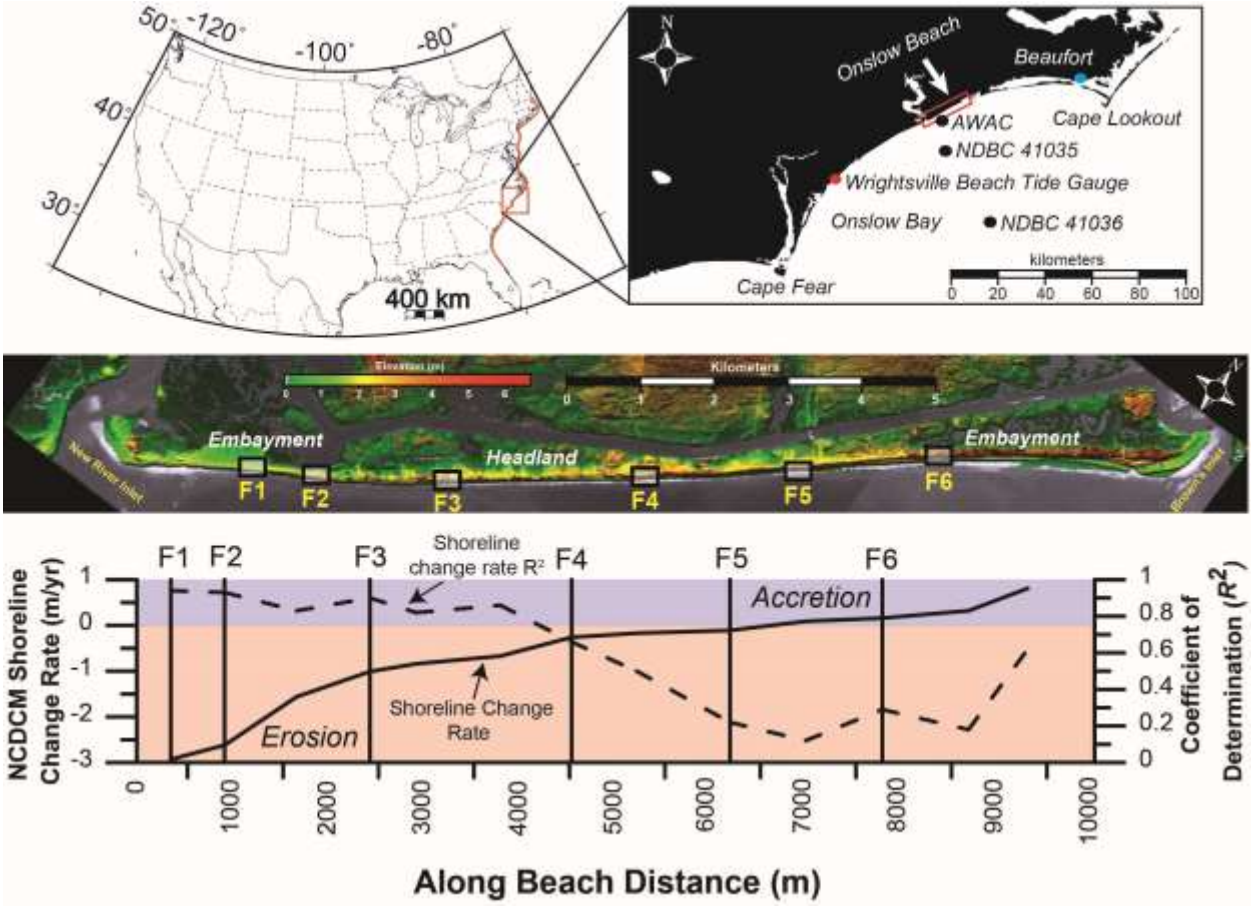

(Top) Study area map showing locations of the NOAA Wrightsville Beach (red dot) and Beaufort (blue dot) tide gauges, Acoustic Wave and Current profiler (AWAC), and NOAA data buoys. NOAA data buoys were used to fill wave-data gaps in the AWAC record. The geographic extent of the NOAA-reported 2009 sea level anomaly is shaded red. (Middle) Hill-shaded topographic map highlights the variable morphologies along Onslow Beach and the locations of the six focus sites. (Bottom) Decadal shoreline change rates for Onslow Beach (Benton et al., 2004).

time scales. Onslow Beach enables exploration of the impacts from sea level anomalies on different beach morphologies and shoreline trajectories that are minimally confounded by spatial differences in hydrodynamic processes, making results from this study applicable to many other beaches. We selected six focus sites for data collection, each extending from the dune line to 0.0m NAVD88 (North American Vertical Datum of 1988) and are 150 m wide in the along-

beach direction. Three of the focus sites (F1, F2, and F3) are in the southwest transgressive section of the island, while the other three (F4, F5, and F6) are in the northeast aggradational section (Figure 1.1).

Waves predominantly approach Onslow Beach from the south, and the prevailing wind direction during the summer and winter is from the southwest and northeast, respectively (Rodriguez et al., 2013). Onslow Beach is impacted by tropical systems in the summer and fall and extratropical systems in the winter (nor'easters). Tidal variations at Onslow Beach are ~1 m. Long-term sea level rise in Onslow Bay is ~3.71 ± 0.64 mm/yr, as measured over 27 years at the NOAA tide gauge in Beaufort, NC (Zervas, 2001). Water levels vary seasonally, as they do along the entire U.S. East Coast, in response to the steric cycle of oceanic heating and cooling. Specifically, there is a water level maximum along the U.S. East Coast in September and a minimum in March (Hong et al., 2000; Sweet et al., 2009).

While coastal erosion in response to accelerated sea level rise may be more prominent north of Cape Hatteras, erosion in response to sea level anomalies should affect areas south of Cape Hatteras as this region is strongly connected to changes in Gulf Stream transport (Sallenger et al., 2012; Ezer, 2013). Sea level anomalies along the U.S. East Coast, including Onslow Beach, are primarily forced by northeasterly winds and reductions in transport strength of the Florida Current, which becomes the Gulf Stream (Sweet et al., 2009). Northeasterly winds can raise coastal sea level through Ekman-driven onshore transport and by slowing the Florida Current (Sweet et al., 2009). The Florida Current transport and water surface gradient in the Gulf Stream are in geostrophic balance yielding a cross-stream water level gradient that increases as the transport increases and an inverse relationship between transport and coastal sea level along the U.S. East Coast. The connection between Florida Current transport and coastal sea level is

most pronounced south of Cape Hatteras, which is ~175 km north of Onslow Beach. Sea level anomalies are often geographically extensive with one event extending over large stretches (>100's km) of coastline. Sweet et al. (2009) documented a sea level anomaly that occurred in June and July of 2009 across most of the U.S. East Coast from Massachusetts to Florida, which coincided with a perigean-spring tide to produce extensive coastal flooding.

3. Methods

Beach profiles are commonly used for evaluating volume changes to beaches; however, the results are sensitive to the hydrological and meteorological conditions around the sampling day, as well as where the profiles are located with respect to the beach morphology (Robertson et al., 2007; Theuerkauf and Rodriguez, 2012). To minimize the contingency introduced by profiles, we assessed beach erosion by measuring the annual Maximum Depth of Erosion (MDOE) (Rodriguez et al., 2012). In addition, the challenge of timing data collection before and after storms and sea level anomalies, which are difficult to forecast and plan around, is mitigated by measuring the MDOE.

The MDOE was measured using methods outlined in Rodriguez et al. (2012) and summarized below. Each February from 2009 to 2012 we sampled all six focus sites along Onslow Beach in one day during the 3 h before and after low tide to ensure similar hydrographic conditions during data collection. We collected six cores from each site each year using a jackhammer. Core locations and elevations were surveyed with an RTK-GPS. Two transects separated by ~40m were occupied per site, and cores were collected at fixed locations along those transects based on the morphology of the beach in 2009 (mid intertidal, high intertidal, and backshore), resulting in 36 cores per year and 144 cores in total for the entire study. Beach profiles were collected using the RTK-GPS (0.25m spacing between points) along each core

transect from the dune toe to the lower intertidal part of the beach to calculate width and gradient (Appendix 1.1). Gradient was measured as rise over run along the profiles from the dune toe to the mean high water shoreline (0.36m NAVD88) (Weber et al., 2005).

Prominent lithologic contacts and beds recognized at depth between pairs of successive cores (e.g., 2009 and 2010) were matched. The elevation offset or depth of bedding-pattern mismatch between the two time periods is the MDOE, which can also be interpreted as the lowest elevation of the beach at that coring location for the preceding time period (Rodriguez et al., 2012). Error in the MDOE measurement is ~ ±2.5 cm, which is calculated as the sum of a ±1.5 cm average GPS error and a ±1 cm lithologic contact measurement error. Sediment compaction from the coring process was not measured. It is assumed to be constant among consecutive cores and, if present, would underestimate the true MDOE. The MDOE method integrates all erosion during a given period, caused by either one large erosive event (e.g., hurricane) or the sum of many smaller high-frequency erosive events. Cores were collected at approximately the same coordinates each year (~3 cm from the initial core location per subsequent year), making it unlikely that those small differences in core locations cause significant vertical displacement of bedding. At some sites the transgressing shoreline caused the beach zones to migrate landward. To account for this, if a beach zone shifted permanently landward over the adjacent core, the core was considered to be collected in the new zone for the MDOE calculation. For example, at Site F2, the backshore in 2009 shifted to high intertidal in 2010 and 2011; thus, those cores were labeled backshore for the MDOE from 2009 to 2010 but high intertidal for 2010 to 2011 with no backshore zone being sampled that year. Where the MDOE was deeper than we could sample, it was reported as a greater-than value.

Hourly water-level data relative to mean sea level (MSL) were analyzed to identify sea level anomalies (Figure 1.2). Water-level data from the Wrightsville Beach National Oceanic and Atmospheric Administration's (NOAA) tide gauge for the entire length of the record at this site (August 2004 through February 2012) were retrieved from the NOAA-Center for Operational Oceanographic Products and Services website (http://tidesandcurrents.noaa.gov). The water level gauge is located at the end of the Johnny Mercer Pier (34° 12.8′ N, 77° 47.2′ W) in Wrightsville Beach, NC ~60 km southwest of Onslow Beach, and measurements are assumed to be relevant to the study area given their proximity within Onslow Bay (Figure 1). This assumption is supported by a strong correlation between water-level data from Wrightsville Beach and Beaufort, NC, which is located ~120 km away on the opposite end of Onslow Bay ($r = 0.964$). The residual between observed and predicted water levels was detrended to remove longer term relative sea level rise and filtered using a 30 day low-pass filter (Figure 2). Those filtered residuals were used to identify sea level anomalies, which we define as occurring when the amplitude of the elevated water level residual is higher than 1 SD from the long-term mean (August 2004 through February 2012) over a period longer than a weather event (2 weeks) but shorter than a seasonal event (anomaly threshold = 0.0819m relative to MSL; Figure 1.2). To compare these data with the MDOE sampling intervals (~1 year) the percentages of water level observations identified as anomalies over those intervals were computed.

To quantify wave conditions, an Acoustic Wave and Current profiler (AWAC) was deployed offshore of Onslow Beach in ~7.5m of water (Figure 1.1). The instrument provided a nearly continuous record of significant wave height (Hs) data from March 2008 through November 2011; however, since the instrument was taken offline several times for repairs and as our beach erosion data extends through February 2012, Hs data from adjacent NOAA National

Data Buoy Center (NDBC) buoys (Onslow Bay Inner-41035; Onslow Bay Outer-41036; http://www.ndbc.noaa.gov) were utilized to fill in data gaps (Figure 1.2). Gaps (~14% of the total wave record) were filled using a Model II linear regression, which was required because the variables on both axes were measured with error (Sokal and Rohlf, 2012), between AWAC and buoy data (Appendix 1.2). For example, the AWAC data gap between February and April 2011 was filled by transforming Hs data from the inner buoy using an equation derived from regression analysis between contemporaneous AWAC and inner buoy data from February through April from other years in the study. Data gaps were preferentially filled with inner buoy data; however, when that buoy was offline, the same transformation method was used with the outer buoy. For analyses, the observations above the Hs mean (0.724m) and above an extreme Hs threshold (1.56 m) were examined separately for each of the beach surveying time periods. The extreme Hs threshold was defined as those Hs values greater than the highest 2% of all Hs values, which is a commonly used extreme value cutoff (Holman, 1986).

4. Physical Forcing

The summer of 2009 through March of 2010 was a period of frequent sea level anomalies, with six events including three of the longest duration and highest amplitude in our record (Figure 1.2). During the first beach sampling year (February 2009 through February 2010), 40% of the water-level observations were anomalies, which is greater than 2010–2011 (8.2%) and 2011–2012 (9.6%). The sea level anomaly in June and July of 2009, recognized by NOAA along most of the U.S. East Coast from Florida to Massachusetts (Sweet et al., 2009), was recorded in Onslow Bay as the third highest and second longest duration in our study (Figure 1.2).

Figure 1.2:

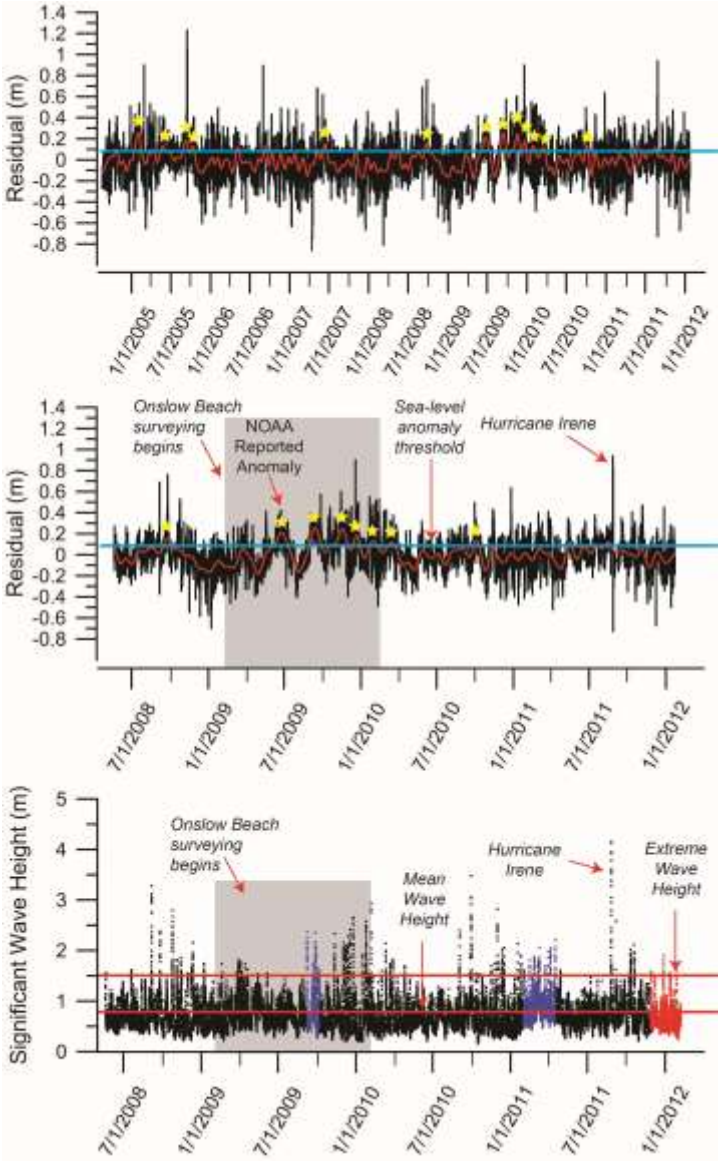

(Top) Residual between the observed and predicted water-level values for the entire record at Wrightsville Beach (August 2004 through February 2012). Unfiltered water-level data are in black, and the filtered data are in red. Sea level anomalies are annotated (stars) above the blue line marking one standard deviation above the average filtered residual water levels. (Middle) Water level data corresponding with beach surveys at Onslow Beach. (Bottom) Significant wave height data collected from an Acoustic Wave and Current profiler (AWAC) and two NOAA data buoys (NDBC 41035 and NDBC 41036). Black, blue, and red data points are from the AWAC, inner buoy, and outer buoy, respectively. Mean and extreme significant wave heights are denoted by the red lines. Hurricane Irene is annotated, and the interval with increased frequency of sea level anomalies is indicated by the gray box in panels 2 and 3. Details on the model used to transform the offshore NOAA-buoy data can be found in Appendix 1.2.

During the year with frequent sea level anomalies (2009–2010) no large storm events with Hs exceeding 3.0m occurred at Onslow Beach (Figure 1.2). Only one sea level anomaly and one storm with a maximum Hs of ~3.0m occurred at Onslow Beach from 2010 to 2011, which we label as a "low-events year." The largest significant wave heights recorded during the study were associated with Hurricane Irene in August of 2011 (maximum Hs = 4.15 m), and we label the beach-sampling period from 2011 to 2012 as a "hurricane year." Irene was a Category 1 hurricane when it made landfall near Cape Lookout, NC on August 27 and produced a storm surge of ~2m above NAVD88 at a pier ~10 km south of Onslow Beach (McCallum et al., 2012).

The percentage of wave observations greater than the mean Hs (2009–2010: 43.4%; 2010–2011: 36.1%; and 2011–2012: 47.3%) and greater than the extreme Hs (2009–2010: 2.5%; 2010–2011: 1.6%; and 2011–2012: 1.9%) does not vary greatly among these "event" periods. This suggests that waves were not consistently higher during any of the sampling periods. To test this more rigorously, we used one-way analysis of variance (ANOVA) to compare significant wave heights among each of the periods for just the mean to extreme Hs and, separately, for the extreme Hs. Preliminary examination of both data sets indicated significant autocorrelation of the Hs data. Consequently, we subsampled each data set (separately, n = 1500 for mean to extreme Hs and n = 300 for extreme Hs) and ln-transformed the subsets to remove autocorrelation, have normally distributed data, and meet assumptions of ANOVA. There were no significant differences among event periods in either data set (mean to extreme Hs, $P = 0.67$, and extreme Hs, $P = 0.85$). Overall, late autumn and winter have higher percentages of extreme waves than the other seasons due to the occurrence of nor'easters. Although there were several winter nor'easters in 2010, the higher number of extreme Hs observations during that winter

(October 2009 to February 2010) did not, as indicated above, affect the mean Hs among the event periods.

5. Effects of Sea Level Anomalies on Onslow Beach

To relate the effects of the sea level anomalies and Hurricane Irene on beach morphology we assumed that the dominant event during a given sampling period is primarily responsible for the observed MDOE. This assumption is reasonable for the MDOE method because it is unaffected by accretion and records the maximum erosion that occurred during the period. Hs values were not significantly larger from 2009 to 2010 than the other sampling periods and there were no named storms; thus, the frequent sea level anomalies are assumed to be the main facilitator for erosion. The anomalies increased the duration and extent of wave energy impacting the beach, which resulted in erosion. From 2010 to 2011 there were no named storms and only one sea level anomaly. Erosion during that year resulted from the few wave events that impacted Onslow Beach, which were likely associated with nor'easters. Erosion measured from 2011 to 2012 is likely the result of Hurricane Irene because other than that storm, wave energy was relatively low and only two low duration and low-magnitude sea level anomalies occurred. Although the highest storm surge would have occurred north of Onslow Beach, a post-storm field excursion revealed that washover terraces and fans formed along the southern and central potions of the island. Those features indicate that during the storm the island was heavily impacted by wave runup.

The average backshore, high intertidal, and mid-intertidal MDOE values during the year with frequent sea level anomalies were ~25, 50, and 55 cm, respectively (using minimum values when cores were not long enough to measure the MDOE). These average MDOE values are

Figure 1.3:

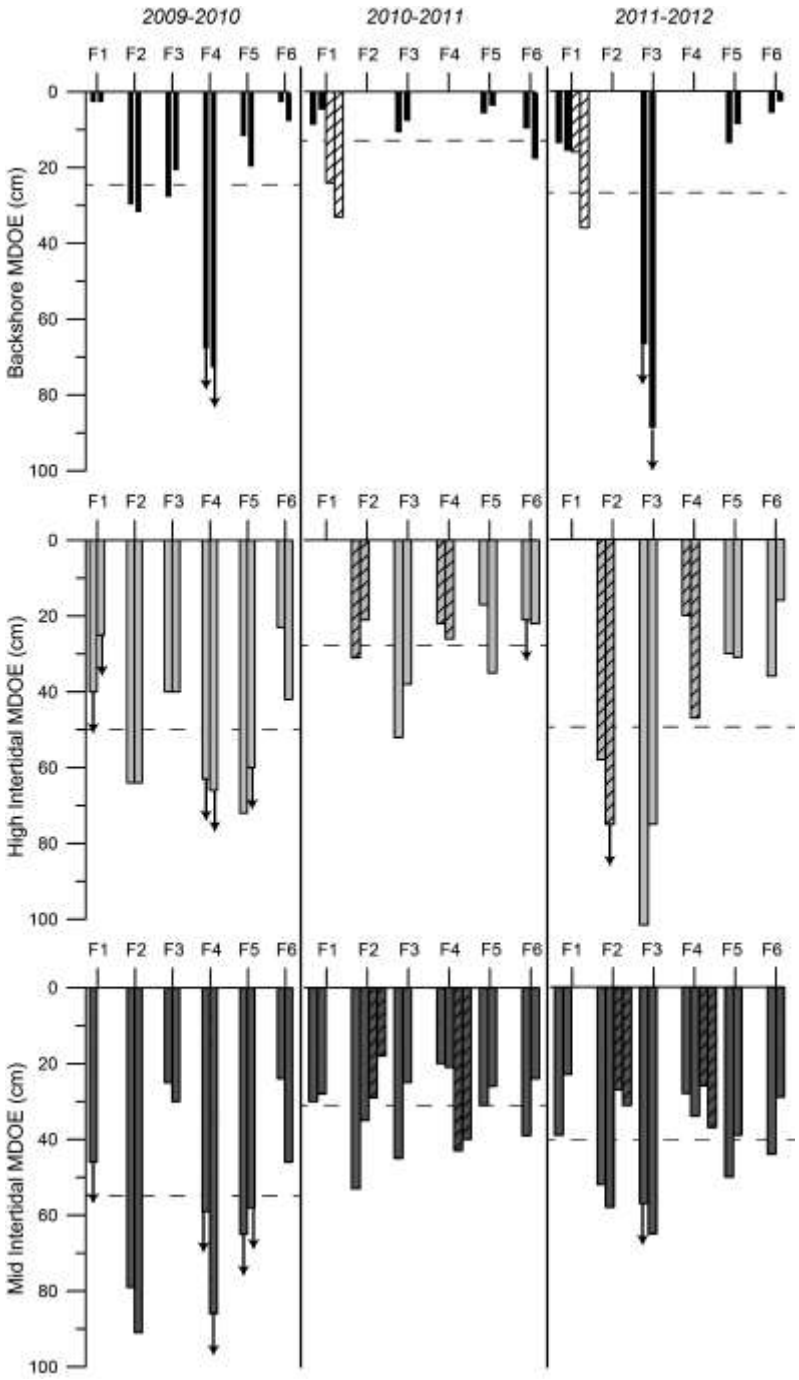

The annual Maximum Depth of Erosion (MDOE) at each beach zone and site for this 3 year study (2009–2010: frequent sea level anomalies; 2010–2011: low-event year; and 2011–2012: hurricane year). The dashed line shows the average annual MDOE at each beach zone. Downward pointing arrows indicate that the MDOE was greater than the core depth. Hatches are used to highlight an instance where beach morphology changed and the zone the core was collected in shifted; for example, the backshore at F2 transitioning to high intertidal after 2010.

greater than those measured during the low-events year (~13, 29, and 32 cm) and similar to the storm year (~27, 49, and 40 cm; Figure 3). The average MDOE during the year with frequent anomalies includes 12 observations that were too high to measure (reported as minimum values), as compared to only one observation during the low-events year and four observations during the storm year. The true magnitude of the MDOE during the year with frequent anomalies is difficult to quantify because one third of the observations are minimum values; however, the MDOE was generally greater that year than what we measured during the subsequent 2 years. Comparing the MDOE at each beach zone between years illustrates how sea level anomalies and storms affect different areas of the sites, and how erosion varies with beach morphology.

Each year of this study, the MDOE roughly followed changes in the beach gradient, with the highest MDOE in the middle of the island along the headland where the beach gradient is steepest, and the lowest MDOE in the embayments where the gradients are lowest (Appendix 1.1 and Figure 1.3). This was observed at Onslow Beach by Rodriguez et al. (2012) and was attributed to the higher wave energy that impacts steeper beaches (plunging breakers) than lower-gradient beaches (spilling breakers). The pattern is evident in all of the zones in the low-events year and is exacerbated during years with frequent sea level anomalies and a storm.

High backshore erosion occurred at the central Onslow Beach sites (F2–F4) in the year with frequent sea level anomalies (Figure 1.3). Morphologic changes at sites F2 and F4 were so dramatic that the backshore transitioned to high intertidal and the high intertidal transitioned to mid intertidal at these sites during that first year and remained in this configuration throughout the subsequent years (i.e., never recovered). The anomalies likely focused wave energy on the backshore and high intertidal of F2 and F4 given the steep and narrow morphology of the beach

at these sites. The backshore at Site F1 accreted seaward during the year with sea level anomalies. That unique response was likely the result of short-term shifting of the ebb-tidal delta shoals associated with the New River Inlet because we observed seaward shoreline movement from Site F1 south to the inlet during 2007–2011. All sites (except F3) experienced similar or greater MDOE at the high intertidal zone during the year with frequent sea level anomalies than the year with Hurricane Irene (Figure 3). The MDOE of the mid-intertidal zone was deeper during the year with frequent anomalies at all of the sites except F3 and F6 (Figure 3). The relatively low MDOE measurements across all of the zones at Site F3 during the year with the frequent sea level anomalies and the high MDOE at that site during the hurricane year are inconsistent with adjacent sites. This is likely due to shallow muddy back-barrier deposits present below the foreshore that are resilient to erosion and occasionally crop out at that site (Rodriguez et al., 2012). Unlike sandier adjacent sites, erosion of the back-barrier unit at F3 requires a high-energy storm event, such as Hurricane Irene. The sea level anomalies coincided with lower wave-energy events; however, they persisted for much longer than a hurricane, which resulted in deep erosion at the sandy sites, but the more resistant back-barrier deposits at F3 were less affected. The MDOE at Site F6 was similar each year of the study and relatively low. Site F6 is not easily eroded by events such as storms and sea level anomalies because it is located in the aggradational section of the barrier where sediment supply is greater due to the landward transport of offshore sand deposits, which are absent south of F5 (Riggs et al., 1995).

6. Conclusion

Sea level anomalies are important facilitators of shoreline erosion but are not included in most models of shoreline response to climate change. Sea level anomalies are linked to the strength of the Gulf Stream (Ezer et al., 2013); thus, variability in Gulf Stream transport induced

by climate change (Sallenger et al., 2012; Ezer, 2013) may result in more frequent and/or higher magnitude anomalies. In addition, meteorological phenomena, such as variations in wind forcing and atmospheric pressure changes, can also result in sea level anomalies. Long-term coastal erosion is punctuated by week- to month-long sea level anomalies, which are shown in this study to enable a large amount of erosion despite not being associated with large storm events (Hs>3 m). At most sites, the erosion in the year with frequent anomalies was similar to or greater than the erosion in the year with Hurricane Irene. Periods with frequent anomalies are not uncommon; throughout the 8 year water-level record at Wrightsville Beach there was one additional period with frequent anomalies in 2005 with ~37% of the observations recorded as anomalies.

In addition to considering impacts from storms and eustatic sea level rise in projections of shoreline erosion, successful coastal management should include sea level anomalies in future planning, as well as how morphologic variations (e.g., beach gradient, and width) and underlying geology influence beach response. Higher gradient beaches, such as those in the center of Onslow Beach, are vulnerable to both storms and sea level anomalies because the wave energy and higher water levels are focused higher on the beach. Underlying geology controls, in part, the variable erosion of a site in response to anomalies because a beach that is underlain by clay at a shallow depth will not erode as easily as a beach where the entire shoreface is composed of unconsolidated sand.

Erosion that results directly from sea level anomalies can increase the vulnerability of a barrier island to overwash and storm erosion if the beach does not rapidly recover. Given that most of the sites at the morphologically variable Onslow Beach eroded during the year with frequent sea level anomalies, it is likely that anomalies influence erosion of sandy beaches worldwide, but the U.S. East Coast may be more prone to large anomalies than other regions due

to the influence of the Gulf Stream (Sweet et al., 2009; Ezer et al., 2013; Ezer, 2013). Sea level anomalies will exacerbate the effects of sea level rise and changes in storm intensity and frequency resulting in increased beach erosion, rates of shoreline transgression, increased demand for limited beach nourishment material, and associated impacts to coastal communities, economies, and infrastructure.

CHAPTER 2: CARBON EXPORT FROM FRINGING SALTMARSH SHORELINE EROSION OVERWHELMS CARBON STORAGE ACROSS A CRITICAL WIDTH THRESHOLD[2]

2.1. Introduction

Blue carbon habitats, such as saltmarshes, mangroves, and seagrass beds, have a tremendous capacity to capture and store carbon dioxide from the atmosphere (Murray et al., 2011). These coastal habitats occupy an order-of-magnitude lower percentage of total global habitat area than terrestrial environments, but have greater carbon burial rates (Chmura et al., 2003; Duarte et al., 2005; Houghton, 2007). Saltmarshes have the highest carbon burial rate per unit area of all blue carbon habitats with a mean of 244.7 ± 26.1 g C m^{-2} yr^{-1} (Ouyang and Lee, 2014), which is greater than long-term burial rates from temperate, tropical, and boreal forests, which range from 0.7 to 13.1 g C m^{-2} yr^{-1} (Schlesinger, 1997; Zehetner, 2010). Saltmarshes occur globally in a variety of settings including fringing the margins of estuaries (fringing marsh), perched on top of relict tidal delta sand bodies (marsh islands), or in river deltas (Berelson and Heron, 1985; Roberts, 1997; Roman et al., 2000). Carbon storage in saltmarshes can be used to offset CO2 emissions from greenhouse gases, provided that marsh accretion keeps pace with sea-level rise. Accelerating sea-level rise will create more accommodation space for marsh growth and could potentially increase carbon sequestration with time (Crooks et al., 2011; McLeod et al., 2011). However, if the rate of relative sea level rise is too high, or if there is not ample

[2] This chapter previously appeared as an article in Estuarine, Coastal and Shelf Science. The original citation is as follows: Theuerkauf, E.J., Stephens, J.D., Ridge, J.T., Fodrie, F.J., and Rodriguez, A.B, 2015. Carbon export from fringing saltmarsh shoreline erosion overwhelms carbon storage across a critical width threshold, *Estuarine, Coastal and Shelf Science*, 164, 367-378.

sediment supply, then the marsh may retreat landward or drown (Morris et al., 2002; Kirwan et al., 2010; Mariotti and Carr, 2014). Conservation and restoration of marshes is a management priority given their importance as carbon sequestration sites as well as the variety of additional ecosystem services they provide, such as buffering storm-wave energy, providing nursery habitat for juvenile fish, and nutrient cycling (Peterson and Turner, 1994; Gedan et al., 2009; Barbier et al., 2011; Moller et al., 2014).

2.1.1. Saltmarsh carbon storage

Carbon is buried in the saltmarsh over annual to decadal time scales within living aboveground and belowground biomass and the trapping of allogenic carbon from the water column (Leonard and Luther, 1995). Sources of biogenic carbon in a saltmarsh include: grasses (e.g. Spartina alterniflora, Juncus roemerianus), benthic algae, and bacteria (Ember et al., 1987). Terrestrial carbon sourced from runoff during high rainfall events as well as phytoplankton and microphytobenthos in the estuary are potential allogenic sources of carbon to saltmarshes (Ember et al., 1987; Middelburg et al., 1997; Gebrehiwet et al., 2008). The inventory of buried organic sediment increases through time as marshes accrete vertically with rising sea level and some portion of the buried carbon is sequestered over millennia in marsh strata after microbial degradation (McLeod et al., 2011; Chmura, 2013). Therefore, carbon burial refers to the buildup of carbon across the marsh surface to some shallow depth; whereas carbon sequestration is the fraction of this carbon that remains stored at greater depths in marsh strata. We define carbon storage as the combination of both burial and sequestration, thus storage represents the time-averaged accumulation of carbon, measured from the marsh surface to the base of the marsh unit and extrapolated across an area of the marsh.

2.1.2. Saltmarsh carbon export

Previous work on the saltmarsh carbon cycle focused on marsh accretion and associated carbon burial and sequestration (e.g. Mudd et al., 2009; Kirwan and Mudd, 2012; Morris et al., 2012). Saltmarshes are being lost globally at alarming rates (Duarte et al., 2008; Duarte, 2009; Nelleman et al., 2009); therefore, carbon export needs to be assessed and included in order to create more accurate saltmarsh carbon budgets. Marsh loss is occurring rapidly in locations such as Louisiana and Chesapeake Bay, where the rates of loss are 43 km^2 per year and 270 m^2 per year, respectively (Wray et al., 1995; Couvillion et al., 2011). Around 25% of the global area originally covered by saltmarshes has been lost, and current loss rates in North America are around 1-2% per year (Bridgham et al., 2006). These losses are occurring in response to a variety of natural and anthropogenic forces, such as climate change (i.e. marsh drowning and erosion in response to accelerated sea-level rise; De Laune et al., 1990; Nicholls et al., 1999; Allen, 2000), human disturbances (e.g. modifications to river systems, deforestation and agricultural reclamation; Day et al., 2000; Pendleton et al., 2012; Ganju et al., 2013; Kirwan and Megonigal, 2013), and wave induced shoreline erosion (FitzGerald, 2008; Mariotti and Fagherazzi, 2013; Leonardi and Fagherazzi, 2014; McLoughlin et al., 2015). Global estimates of carbon released by saltmarsh land-use change are large, ranging from 0.02 to 0.24 Pg CO_2 yr^{-1} (Pendleton et al., 2012), and these estimates are conservative because they do not include direct measures of erosion, which can release sequestered carbon rapidly on event time scales (Coverdale et al., 2014).

Shoreline erosion is suggested to be the principle natural mechanism for current global saltmarsh loss (Schwimmer, 2001; van de Koppel et al., 2005; Gedan et al., 2009; Mariotti and Fagherazzi, 2010; Marani et al., 2011), and erosion is progressing at alarming rates in response to relative sea-level rise, human activities (e.g. boat wakes), and currents and waves

(Schwimmer, 2001; van der Wal and Pye, 2004; Mariotti and Fagherazzi, 2010). In some locations, rates of shoreline erosion are an order of magnitude greater than platform accretion rates (Mattheus et al., 2010). This suggests that carbon export via shoreline erosion could eventually outpace carbon storage, especially if the depth of erosion is equal to or greater than the thickness of the marsh. Even healthy marshes that are keeping up with sea-level rise and transgressing landward may narrow due to rapid shoreline erosion (Reed, 1995; Temmerman et al., 2004), which will reduce the area of the marsh available for carbon storage. A transition in saltmarsh function from a net carbon sink to a source is particularly likely at eroding fringing marshes that are narrowing because upland transgression is impeded by steep topography (Rodriguez et al., 2013) and/or anthropogenic barriers, such as sea walls (Doody, 2004; Pontee, 2013). If a marsh can neither maintain its elevation with respect to sea level, nor migrate landward, it will eventually submerge or lose area, which could result in the export of carbon that has been sequestered in marsh strata and loss of the carbon storage capacity across the marsh platform

The efficacy of a saltmarsh as a carbon storage site depends, in part, on the relative contributions of carbon storage across the saltmarsh platform and erosion at the shoreline. In order to assess how geomorphic change impacts the saltmarsh carbon budget, we developed a box model that estimates the net import or export of carbon to the marsh by comparing carbon storage to shoreline erosion. We then apply this model to an eroding fringing saltmarsh in North Carolina to determine its carbon budget and whether it functions as a carbon sink.

2.2 Methods

2.2.1. Saltmarsh carbon box model

Our model includes both annual estimates of carbon export via shoreline erosion and carbon storage (Figure 2.1). Because the amount of carbon stored per year is scaled to the area of the marsh, in this model, carbon storage decreases as the marsh decreases in width. This is an important component of the model because not only does erosion result in carbon export, but it also limits carbon storage by reducing marsh area. The net annual carbon budget of the saltmarsh, which is the output of this model, can be used to identify the timing and width when carbon export outpaces storage and the marsh transitions to a carbon source (Figure 2.2). Sea-level rise and temperature remain constant in our model simulations in order to isolate the impacts of shoreline erosion on the carbon budget; however, it has been shown that global warming and sea-level rise will likely alter carbon storage and export rates (McLeod et al., 2011; Kirwan and Mudd, 2012).

Figure 2.1: Conceptual model of the estuarine fringing saltmarsh carbon budget

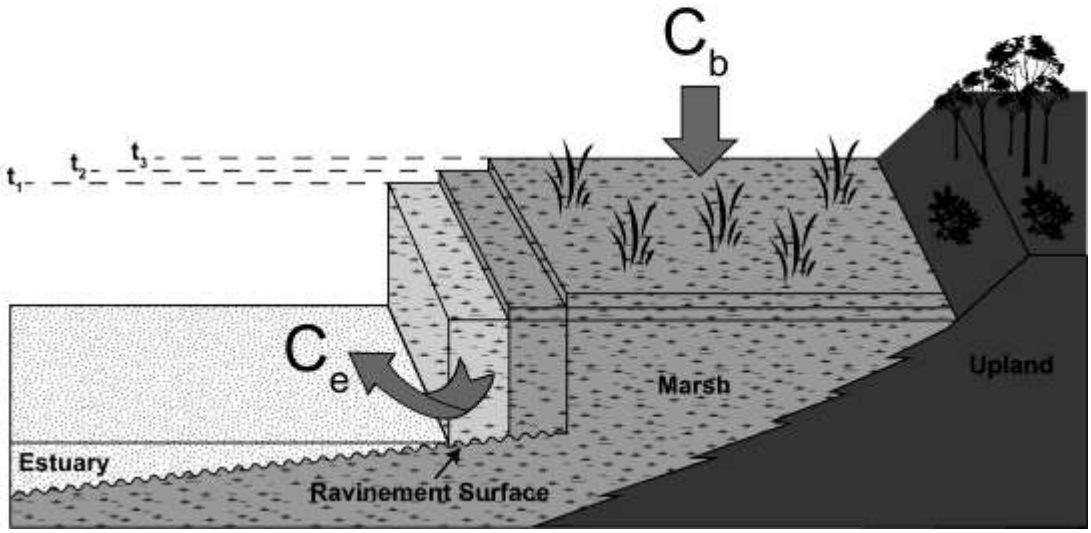

Carbon is stored (C_s) across the marsh platform as the marsh grows upward, and carbon is exported (C_e) into the estuary as the marsh shoreline erodes. In this conceptual model the slope of the upland topography is too steep to allow marsh transgression across the upland, thus the marsh narrows through time.

Figure 2.2: Graphical depiction of the threshold width concept

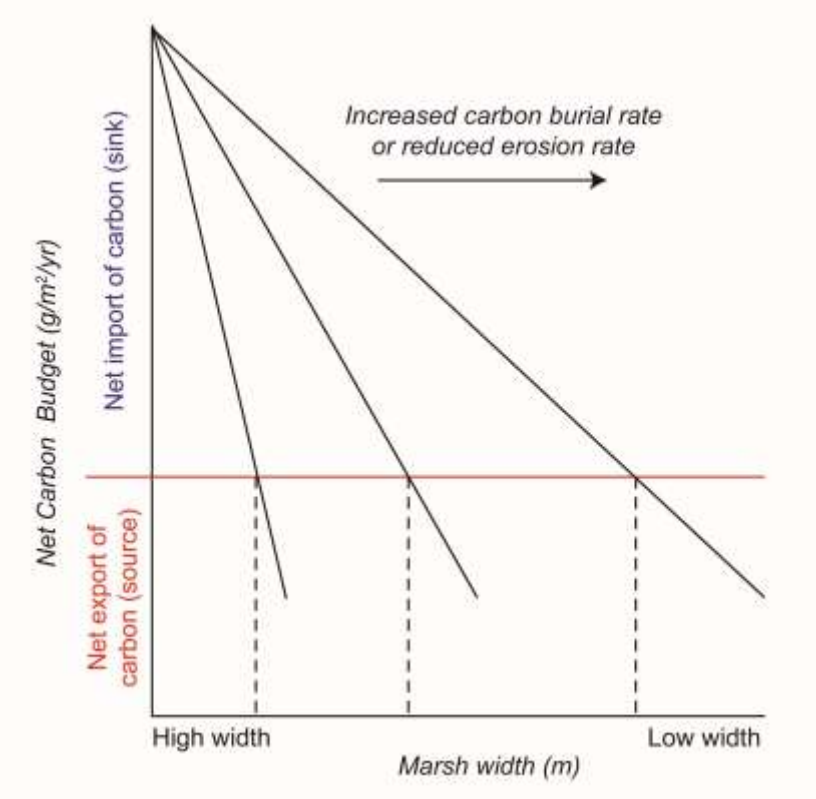

As the marsh narrows in response to shoreline erosion it reaches a threshold width where carbon export exceeds carbon storage and the marsh becomes a source of carbon to the estuary. If the carbon storage rate increases or the erosion rate decreases the threshold width will decrease and the marsh will function as a carbon sink longer. This is demonstrated by the black lines, which depict increasing (decreasing) rates of carbon storage (erosion) from left to right. The vertical dashed lines indicate the threshold width for each scenario.

2.2.2. Parameters and assumptions

This model examines the net annual carbon budget of a saltmarsh (C_n) by differencing carbon storage (C_s; g yr^{-1}) and carbon export (C_e; g yr^{-1}), where positive C_n values indicate net carbon storage and negative C_n values indicate net carbon export (Figure 2.1).

$$C_n = C_s - C_e \quad (1)$$

C_s is a function of the marsh area (M_a; m^2) and the carbon accumulation rate (C_{ar}; g m^{-2} yr^{-1}) and can be expressed using the equation:

$$C_s = M_a \times C_{ar} \quad (2)$$

M_a is calculated for each time step (dt; yr) by summing the initial marsh area (M_o; m^2), the change in marsh area at the shoreline, and the change in marsh area at the upland boundary.

$$M_a = ((dt) \times (L) \times (ds/dt + du/dt)) + M_o \quad (3)$$

The change in marsh area at the shoreline and upland boundaries is equal to the product of the shoreline length (L; m) and the shoreline change rate (ds/dt; m yr^{-1}) and upland transgression rate (du/dt; m yr^{-1}), respectively. The shoreline change rate is negative if the shoreline is eroding (landward movement) and the upland transgression rate is positive if moving landward.

C_{ar} is determined by dividing the marsh carbon inventory (C; g m^{-2}) by the age of the marsh (T; yr) (Choi and Wang, 2004). This takes into account both carbon burial and carbon sequestration. For most marshes, C_{ar} is < the carbon burial rate and > the carbon sequestration rate.

$$C_{ar} = C/T \quad (4)$$

One assumption with this approach is that carbon accumulation is spatially homogenous, while in reality there are a range of accumulation rates across the marsh (Temmerman et al., 2003a). The validity of this approach must be assessed for a particular marsh based on such factors as spatial variations in elevation, vegetation cover, sediment supply, tidal inundation height, and distance from the nearest creek or marsh edge (Connor et al., 2001; Temmerman et al., 2003a; Kulawardhana et al., 2015). An inventory approach is the appropriate method for

deriving the rate of carbon storage because it normalizes the amount of carbon in the marsh through time, taking into account carbon degradation. There is some uncertainty as to whether the inventory approach appropriately accounts for increases in the rate of carbon burial associated with accelerations in sea-level rise and global warming; however, previous research suggests that an increasing carbon pool related to increased burial will result in enhanced decay proportional to the size of the carbon pool (Mudd et al., 2009; Kirwan and Blum, 2011; Kirwan and Mudd, 2012). Using the carbon inventory approach to parameterize the model is not perfect, but does include both recent carbon burial at the top of the marsh unit and older marsh carbon sequestered at depth. The time-averaged carbon storage per year can be calculated using the expanded version of Eq. (2):

$$C_s = [((dt) \times (L) \times (ds/dt + du/dt)) + M_o) \times (C/T)] \quad (5)$$

C_e is the product of the amount of carbon contained within the eroded marsh (E_c; g), L, and ds/dt and is calculated using the equation:

$$C_e = L \times ds/dt \times E_c \quad (6)$$

E_c is determined from the carbon inventory (g m^{-2}) per meter thickness of the marsh at the edge (C/m_t; g m^{-2}), the thickness of the marsh in meters that is eroded (m_e; m), and the amount of carbon accumulation in the marsh during the time step (C_{ar} x dt). This is expressed by the following equation:

$$E_c = ((C/m_t) \times m_e) + (C_{ar} \times dt) \quad (7)$$

Carbon export per year can also be expressed using the expanded version of Eq. (6):

$$C_e = [L \times ds/dt \times ((C/m_t) \times m_e) + (C/T \times dt)]. \quad (8)$$

If the thickness of the marsh at the edge is greater than the erosion depth, then some marsh will be preserved as the shoreline retreats. The model assumes carbon exported via erosion is completely removed from the marsh and does not discern whether the eroded carbon is labile or refractory. The fate of eroded marsh carbon is complex and can follow multiple pathways that are highly dependent on the individual characteristics of an estuary. Some eroded saltmarsh material will be transported back onto the marsh and deposited on the marsh platform. That material is included in the saltmarsh carbon inventory and is likely not transported far into the marsh platform as shown by the work of Temmerman et al. (2003b) and D'Alpaos et al. (2007), which suggests deposition of any eroded material would be proximal to the marsh edge due to marsh grasses baffling flow and inducing sedimentation. Most of the carbon liberated from the saltmarsh, which is relatively young and bioavailable, is respired once it reaches the estuary and is metabolized by microbes (Raymond and Bauer, 2001; Cai, 2011; Canuel et al., 2012). Some of the marsh carbon that is not respired or redeposited in the estuary will enter the open ocean, where it may be remineralized or deposited (Cai et al., 2003). Certainly, the ultimate fate of the eroded carbon will dictate the relative importance of carbon export from marshes for the global carbon budget; however, mitigating the loss of stored carbon in marsh sediments will ensure that fixed CO_2 does not return to the atmosphere.

2.2.3. Study area for model application

We applied the model to a fringing saltmarsh at Carrot Island, which is part of the Rachel Carson National Estuarine Research Reserve in Beaufort, North Carolina (Figure 2.3). Carrot Island is located along the northern shore of Back Sound, is separated from the mainland by Taylor's Creek, and has an extensive fringing saltmarsh along its southern edge with a maximum

cross-shore width of 350 m. The fringing marsh is mainly composed of Spartina alterniflora and is

Figure 2.3: Chapter 2 study area map: Carrot Island, NC

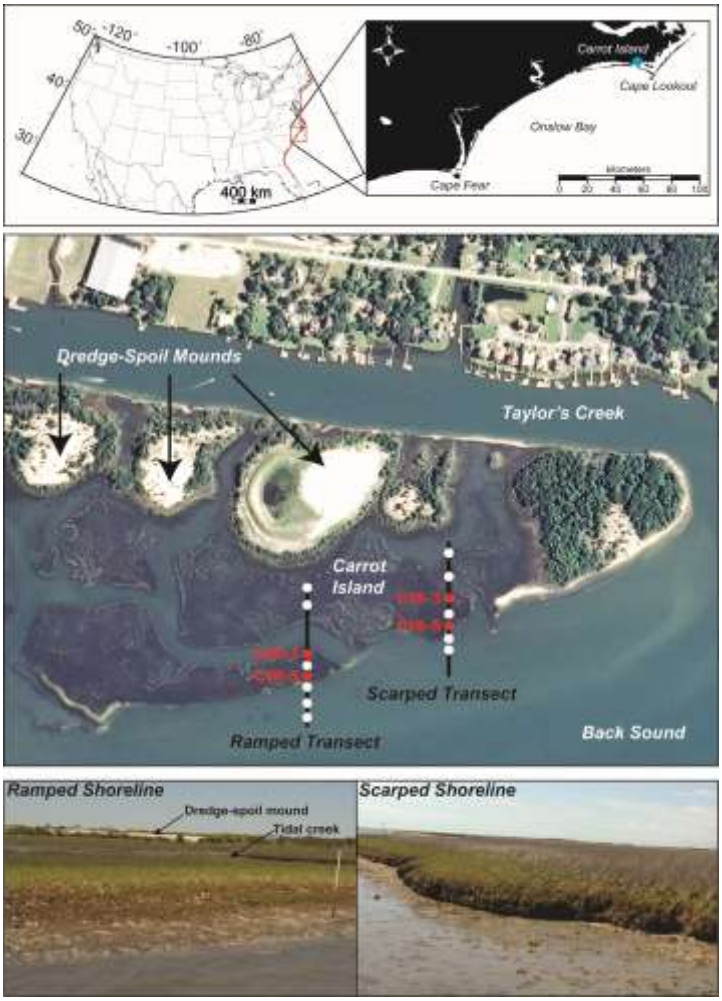

Top panel: Carrot Island is a marsh island in Back Sound, which is located in Eastern North Carolina near Cape Lookout. Middle panel: Zoomed-in image of the saltmarsh at Carrot Island. Circles indicate locations of vibracores collected. Red circles denote cores used to determine the carbon content and the age of the marsh. Bottom panel: Ramped and scarped shoreline morphologies are found along Carrot Island and these correlate with lower and higher rates of shoreline retreat, respectively.

bisected by meandering tidal creeks. Large spoil mounds are located on the landward edge of the marsh and were created during the dredging of adjacent Taylor's Creek, which began in the early

1900s (Figure 2.3). Upland migration of the marsh with rising sea level is prevented by the steep gradient (15% grade) of the dredge spoil mounds and deep (~2 m) Taylor's Creek. Relative sea level is rising ~3.2 mm/yr and land subsidence is minimal (~1.0 mm/yr) at this site based on the Tump Point sea-level curve developed by Kemp et al., 2011, which is < 40 km away from Carrot Island. Carrot Island is micro-tidal and waves are predominantly low in height (<1m) and short in period (1-2 s). The bayward edge of the marsh is subjected to erosive waves from persistent southwesterly winds during the summer, storms (nor'easters and hurricanes), and boat wakes. A series of embayments and promontories characterize the marsh edge and both ramped- and scarped-edge morphologies are evident along the shoreline (Figure 2.3).

2.2.4. Field and laboratory methods

We collected vibracores to sample the saltmarsh and nearshore stratigraphy and used historical aerial photographs to measure changes in marsh area in order to gather inputs for the model. Cores were distributed along shore-normal transects at both the ramped and scarped marsh shorelines from the nearshore in Back Sound, to the landward marsh boundary, adjacent to the dredge-spoil mounds (Figure 2.3). Fifteen cores were collected at Carrot Island to a depth of ~2.0 m below the sediment surface. Elevation data, relative to the North American Vertical Datum of 1988 (NAVD88), were collected using a Trimble 5700 RTK-GPS for each core location as well as every 0.25 m along each transect to measure the depth of erosion, marsh surface elevation, and elevation of stratigraphic units within the cores. The depth of erosion is used to determine how much of the marsh is excavated during shoreline transgression, which ultimately defines the amount of carbon exported into the estuary. The depth of erosion was measured as the distance between the marsh surface at the shoreline and the depth of the shoreface toe, where the bay floor flattens into Back Sound.

Cores were transported to the laboratory, where they were opened, photographed, described, and sampled. Samples were collected to determine the age of the marsh as well as the carbon content and grain-size characteristics of the marsh material and other lithologic units. Marsh age was approximated from radiocarbon dating Spartina alterniflora material sampled from the base of the marsh in cores CIR-5 (Edge, Ramped) and CIS-5 (Edge, Scarped) (Figure 2.3). The assumption with this approach is that the material dated represents the time of initial marsh colonization (Redfield and Rubin, 1962). Only grass blades and stems were sent to Beta Analytic for carbon-14 dating to ensure that the material dated represents the earliest aboveground saltmarsh biomass. An articulated cross-barred venus (Chione cancellata) shell from a lower unit was also sent for dating. The conventional age dates have a reported error of ±30 years and were calibrated using the IntCal09 radiocarbon calibration curve (Reimer et al., 2009).

Cores CIS-3 (Interior, Scarped), CIS-5, CIR-3 (Interior, Ramped), and CIR-5, from the marsh platform, were split into 5-cm sample bins from the top of the core to the base of the marsh unit. Additional smaller samples, 2 cm^2, were obtained from the other units sampled in the cores to help define their environment of deposition. Sediment compositions of all samples were characterized by measuring grain size and organic carbon content. Samples were dried in a low-temperature oven, weighed, and then disaggregated and homogenized with a mortar and pestle. Grain size was measured on subsamples using a Cilas 1180 laser particle-size analyzer, which can measure sediments from 0.04 to 2500 mm. Percent organic carbon in the sediments was measured on subsamples using a Perkins-Elmer CHN analyzer. Error associated with the CHN analyzer and subsampling was quantified experimentally by calculating the average standard deviation of three measurements on subsamples from the same core interval. That was repeated

on three core intervals and the average of those three standard deviations is the error (±0.17%). The amount of carbon in each sample bin (g m^{-2}) was determined by multiplying the percent organic carbon by the sample mass and the inverse of the sample area.

Marsh shoreline erosion rates were determined using georectified United States Department of Agriculture (USDA) aerial photographs from 1958, 1971, 1983, 1989, 1994, 2005, 2010, and 2012. The marsh shoreline was digitized from each photograph as the contact between the living marsh and the water's edge. Distances of each of these shorelines from the oldest shoreline (1958) were used to measure shoreline erosion. A linear regression model was used to calculate the retreat rate and coefficient of determination (R^2) from the measured displacements. Georectifying the aerial photographs and digitizing the contacts are the potential sources of error in the marsh erosion and upland transgression rates and these errors are <0.25 m (Moore, 2000; and references therein).

2.3. Results and interpretations

2.3.1. Sedimentology and stratigraphy

The saltmarsh was sampled as ~50 cm thick and is composed of dark greenish-gray silt (5G 4/1) with high organic-carbon content (1-6% C; Figure 2.4). Overall, percent organic C peaks at a depth of 5-10 cm for the interior cores CIS-3 and CIR-3 and at a depth of 20-25 cm and 25-30 cm for cores CIS-5 and CIR-5, respectively, collected at the marsh edge (Figure 2.4). That peak may correspond with the depth of maximum below-ground biomass or may be the result of autocompaction, and percent organic C gradually decreases to about 1% C below that peak to the base of the marsh. The grain-size distribution is bimodal with peaks at ~30 mm and ~150 mm. The grain size of the marsh sediment in cores CIS-3 and CIR-3, collected landward of

the marsh shoreline, becomes finer at progressively shallower depths in the cores with the major grain-size

Figure 2.4: Lithologic logs, percent organic carbon, and sediment grain size profiles of the cores used to parameterize model at Carrot Island, NC

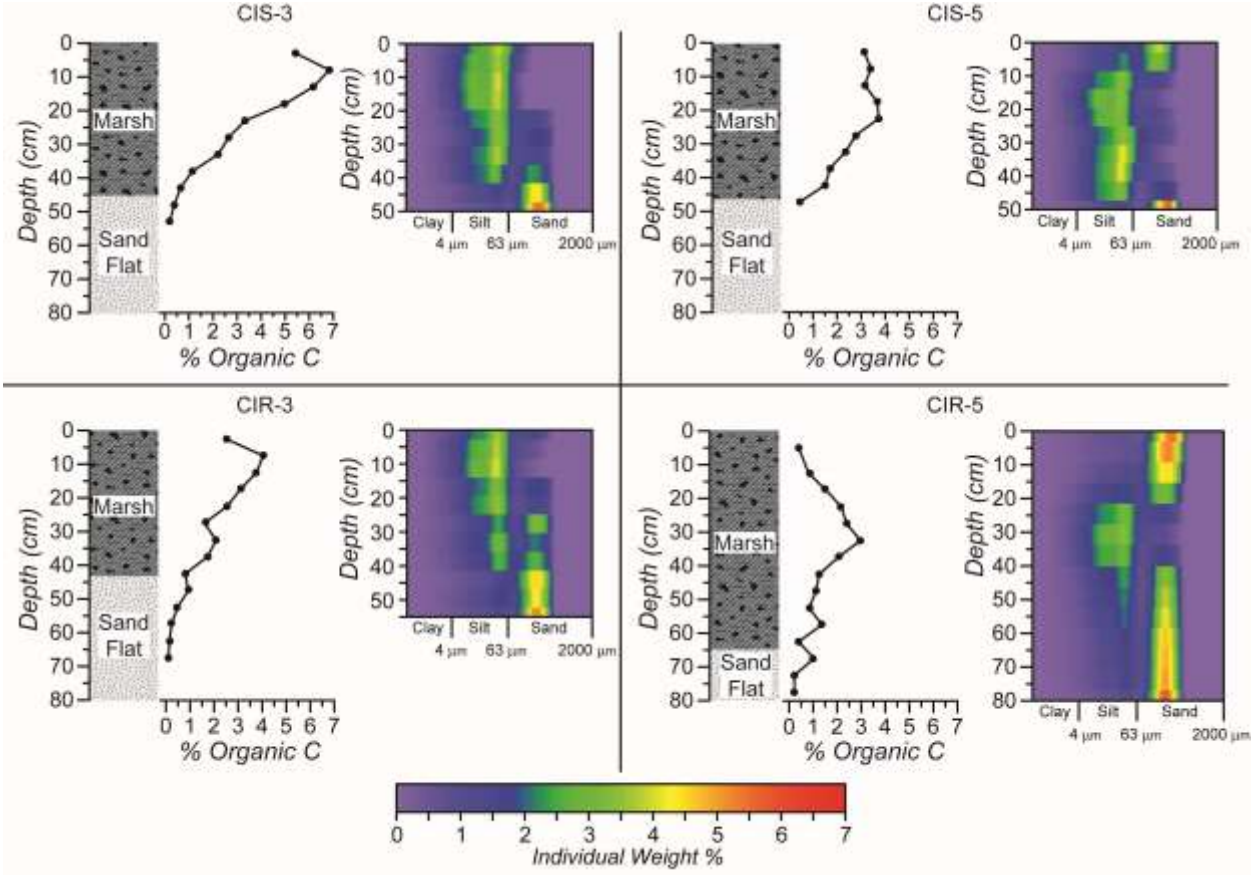

Lithologic logs, percent organic carbon, and sediment grain size profiles of the cores used to parameterize the model runs for Carrot Island. Warmer colors on the grain size profile indicate a higher percentage weight of that particular size class in a sample.

peak being sand at the base of the cores and silt at the top. Cores CIS-5 and CIR-5, collected at the marsh shoreline, show that same general trend, except the top 10-15 cm of the cores are dominated by sand (Figure 2.4). Abundant Spartina alterniflora roots, seeds, and stems, were recognized in the saltmarsh unit, in addition to other woody debris. Below the saltmarsh depositional unit, two other distinct regional lithofacies were sampled.

Many of the cores sampled a stiff, dark gray (N4) poorly sorted silt with a mean grain size of 31 mm to an olive gray (5Y 4/1) poorly sorted clayey sand with a mean grain size of 148 mm at the base. The dark gray silt is bimodal with a dominant silt mode at ~15 mm and a minor sand mode at ~150 mm. In some of the cores, the unit contains interbedded silt and sand. Whole shells and fragments are found throughout the unit and the organic carbon content of the unit is ~1.6% C. Carbon-14 dating of an articulated cross-barred venus shell (C. cancellata) collected at the top of the unit suggests deposition around 1250 to 910 cal yr BP (cal AD 700-1040; Appendix 2.1). This unit is interpreted to have formed in a restricted lagoon environment and was also sampled by Berelson and Heron (1985) below Middle Marsh, located about 1 km southeast of Carrot Island in Back Sound.

All of the cores collected from Carrot Island sampled a medium gray (N5) moderately sorted sand with a mean grain size of 182 mm above the restricted lagoonal unit and below the marsh. This unit extends into Back Sound where it is exposed at the bay floor as a sand flat. Shell fragments are found throughout the unit and the organic carbon content is low (<1% C). The fringing marsh of Carrot Island colonized the sand flat and during high-energy events, sand is transported across the shoreline and deposited at the marsh edge forming a narrow (1e4 m wide) levee < 0.25 m in relief (Figure 2.5).

Other localized lithologic units were sampled at Carrot Island. Core CIR-1, located adjacent to a dredge-spoil mound, sampled coarse sand with shell fragments at the top. This unit is interpreted as dredge-spoil material given its proximity to the spoil mound and that it is overlaying marsh (Figure 2.5). Cores CIS-6 and CIS-7, collected adjacent to the marsh scarp in Back Sound, sampled a thin (~0.25 m) organic-rich unit at the tops of the cores. This unit is interpreted as eroded marsh material since the grain size of these sediments was similar to those

of the marsh unit (bimodal distribution with major peak ~30 mm and minor peak around 150 mm; mean diameter 37 mm). Waves undercut the surface of the marsh creating an overhang, which eventually slumps off, and this process and deposit was previously documented by Schwimmer (2001) and Mattheus et al. (2010).

Figure 2.5: Stratigraphic cross-sections from Carrot Island

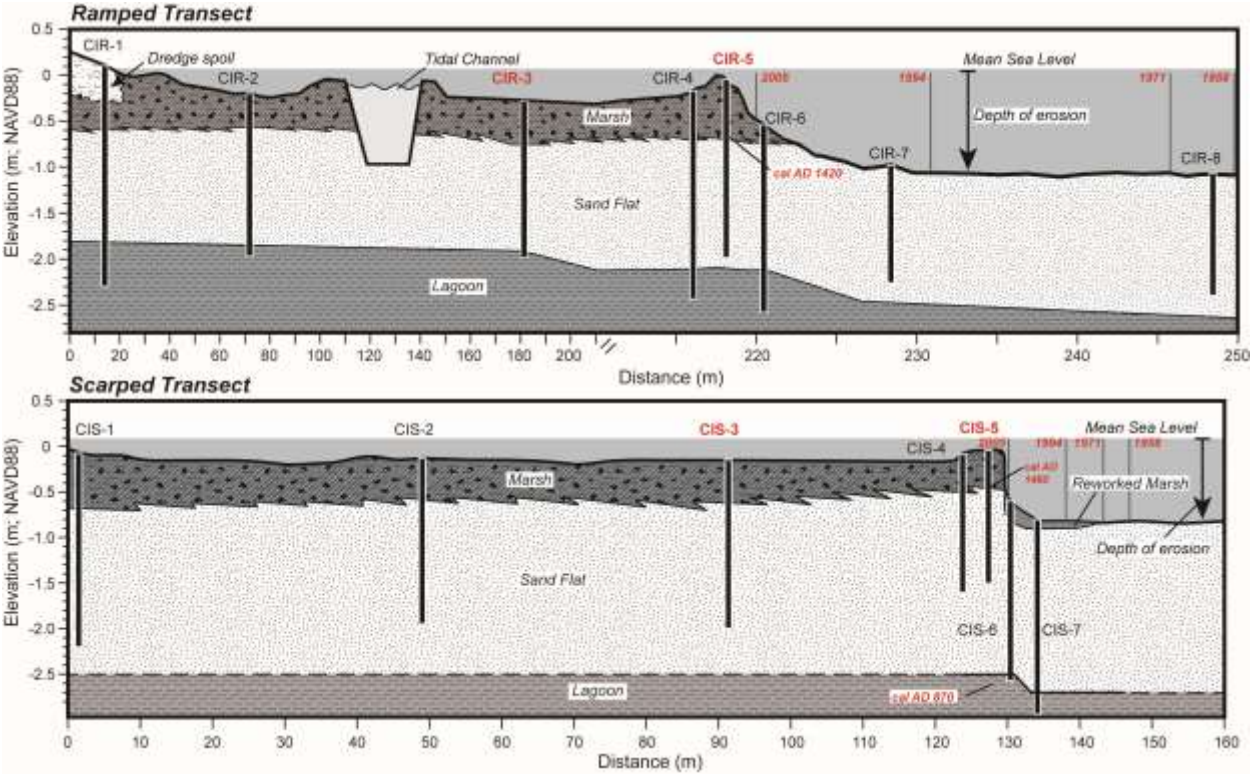

Transect locations are shown in Fig. 3. Cores annotated in red were used to parameterize the model. Locations of former marsh shorelines were determined from aerial photography and are depicted on the cross-sections with the vertical gray lines. Ages of the marsh and lagoonal units measured with radiocarbon dating are also depicted on the cross-sections.

To assess the subsurface geometry of the marsh and erosion depth at the shoreline, we constructed stratigraphic cross-sections using the core interpretations and RTK-GPS data. The general sequence at Carrot Island is a basal lagoonal unit, overlain by sand flat that was colonized by saltmarsh (Figure 2.5). The marsh has a nearly uniform thickness from the

shoreline to the upland margin. Dates of the base of the marsh from cores CIR-5 and CIS-5 along both the ramped and scarped transects were ~1420 cal AD and ~1460 cal AD, respectively (Figure 2.5; Appendix 2.1). Given the similarity between the two age dates and the uniform thickness of the marsh the ages likely apply to the entire marsh, indicating when Spartina alterniflora first colonized the sand flat.

The depth of erosion is greater than the thickness of the saltmarsh at Carrot Island and there was no evidence of marsh material preserved bayward of the marsh edge despite aerial photographs indicating, historically, the marsh extended further into Back Sound (Figure 2.5). Given the lack of preservation of marsh in the nearshore below the sediment-water interface, it is likely that the organic-rich unit sampled near the shoreline of Back Sound, and interpreted as eroded marsh material, was an ephemeral deposit that will be completely eroded and transported further into the estuary and/or onto the marsh-edge levee. Redeposition of eroded marsh material likely only occurs proximally to the marsh edge and does not contribute substantially to marsh platform accretion, which is supported both by previous work on marsh sedimentation patterns (e.g. Reed, 1988; Temmerman et al., 2003b; D'Alpaos et al., 2007), as well as geomorphological indicators at Carrot Island, such as the narrow marsh-edge levee (Figure 2.5).

2.3.2. Shoreline movement

The pattern of shoreline movement through time, at the ramped and scarped sites, was derived using the 1958 shoreline position as a baseline (i.e. the shoreline position in 1958 was defined as zero; Figure 2.6). Both shorelines show a consistent pattern of landward movement, and linear regression retreat rates (reported with the 95% confidence intervals) for the ramped and scarped sites are 0.65 ± 0.07 m yr^{-1} and 0.76 ± 0.125 m yr^{-1}, respectively (Table 2.1). Those rates of shoreline retreat are shown to be relatively constant through time as evidenced by the

high r-squared values of 0.99 and 0.97 for the ramped and scarped shorelines, respectively (Figure 2.6).

Figure 2.6: Decadal shoreline retreat rates at Carrot Island

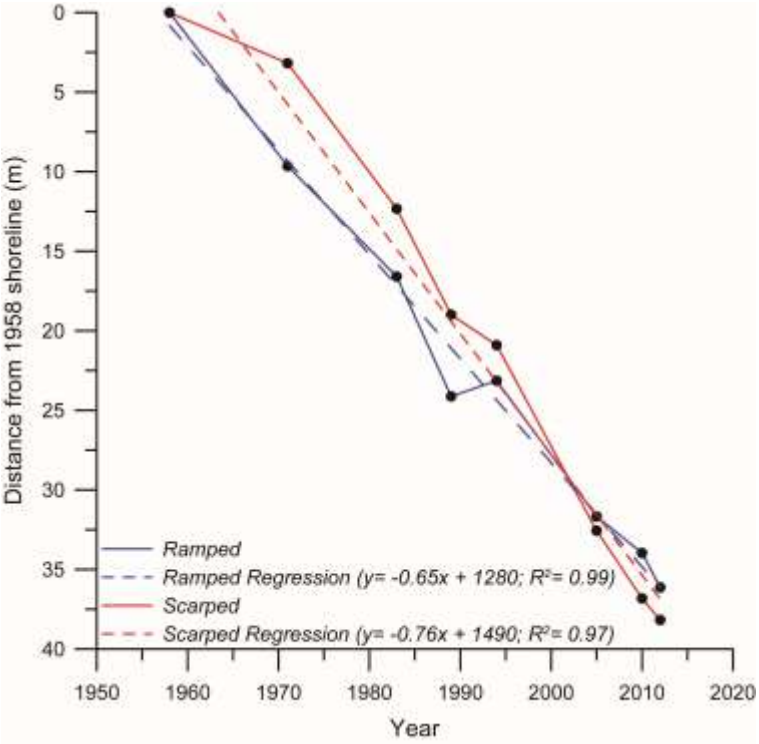

Shoreline positions were determined using aerial photography from 1958 to 2012. The 1958 shoreline was used as the baseline to determine the retreat rates and the distance from this baseline for each subsequent shoreline is plotted on the graph. A linear regression model was used to determine the rate of retreat along each transect.

2.3.3. Parameterizing the model for Carrot Island

We applied the model to the ramped and scarped sites separately, considering their different shoreline-retreat rates. Initial marsh area at both the ramped and scarped sites was 300 m^2, which was determined solely by the marsh width because we used a 1 m shoreline length. The shoreline change rates (ds/dt) used in the model were -0.65 ± 0.07 m yr^{-1} for the ramped site and -0.76 ± 0.125 m yr^{-1} for the scarped site (Table 2.1). The upland transgression rate (du/dt)

was set to 0 because both the steep dredge spoil mounds and deep Taylor's Creek, located behind the marsh, prevent upland transgression and no upland transgression was documented in the aerial photographs. A similar situation exists in areas where development is at the landward edge of the marsh (Doody, 2013; Pontee, 2013). Cores CIR-3 and CIS-3, from the interior part of the platform behind the ramped and scarped shorelines, were used to develop the carbon inventory (C; Table 1). Marsh age (T) for the ramped and scarped transects was 588 ± 15 years and 553 ± 30 years, respectively and measured using the cores collected near the shoreline (Table 2.1, Figure 2.5). For Carrot Island, the assumption that the carbon accumulation rate for the marsh platform is homogenous across the marsh and can be derived from a single core in the transect is supported by the similar carbon inventories measured at both the ramped and scarped sites (~7258 ± 52 g C m^{-2} and ~7111 ± 52 g C m^{-2}, respectively), and the relatively uniform marsh thickness (~0.5 m thick) and age (~550 years) (Table 2.1, Figure 2.5). Other fringing marshes might thin and become younger landward, which would necessitate the collection of additional radiocarbon dates and carbon inventories to correctly tune the model. Clearly, there are spatial variations in the carbon accumulation rate across each transect at Carrot Island (e.g. the tidal channel), but the model treats the marsh platform as one box and is tuned using an "average" accumulation rate. Carbon inventories (C) at the edge of the ramped and scarped sections were measured from cores CIR-5 and CIS-5 and were 5527 ± 52 g C m^{-2} and 8251 ± 52 g C m^{-2}, respectively (Table 2.1). All of the marsh material is being eroded away each year at Carrot Island, thus mt and me are equivalent and equal to 70 cm for the ramped site and 40 cm for the scarped site. Time-averaged carbon storage (C_s) and carbon export (C_e) were solved using the above parameters and Eqs. (5) and (8).

Table 2.1: Parameters used in saltmarsh carbon budget model runs for Carrot Island

Model Parameter	Symbol	Value used in model
Shoreline length (m)	L	1
Timestep (yrs)	dt	1
Initial marsh area (m^2)	M_o	300
Ramped edge retreat rate (m/yr)	ds/dt	-0.65
Scarped edge retreat rate (m/yr)	ds/dt	-0.76
Upland transgression rate (m/yr)	du/dt	0
Ramped interior carbon inventory (g/m^2)	C	7257.73
Scarped interior carbon inventory (g/m^2)	C	7111.25
Ramped edge carbon inventory (g/m^2)	C	5527.01
Scarped edge carbon inventory (g/m^2)	C	7251.15
Ramped marsh age (yrs)	T	588
Scarped marsh age (yrs)	T	553
Ramped marsh thickness at the edge (m)	m_t	0.7
Scarped marsh thickness at the edge (m)	m_t	0.4
Ramped marsh thickness eroded (m)	m_e	0.7
Scarped marsh thickness eroded (m)	m_e	0.4

2.3.4. Net carbon budget and threshold width for Carrot Island

Our model identifies the threshold width, which is the marsh width where carbon export from marsh-shoreline erosion exceeds time-averaged carbon storage (Figure 2.2). At the threshold width, the marsh transitions from being a net carbon sink to a net carbon source. Net carbon in the marsh (C_n) was output for each year and used to determine the threshold width. Errors associated with the threshold width were derived from the measurement errors of the shoreline retreat rate, age, and carbon inventory, evaluated with additional model runs that utilized the upper and lower values (Table 2.2, Figure 2.7). Model output shows that the marsh along the ramped section of Carrot Island is presently a carbon sink, but transitions to a source in

2021 $^{+32}_{-25}$ years at a threshold width of 295 $^{+17}_{-18}$ m (Figure 2.7), assuming that average rates of carbon storage and export will not change in the near future. The marsh along the scarped section is currently a carbon source. Assuming that average rates of carbon storage and export have not changed over the past century, the marsh transitioned from a sink to a source 1930 $^{+40}_{-27}$ years at a threshold width of 363 $^{+34}_{-36}$ m (Fig. 7).

Table 2.2: Uncertainty estimates for model simulations at Carrot Island

	Year (AD)	**Width (m)**
Ramped		
Initial simulation	2021	295
Upper shoreline retreat rate (*m/yr;* -0.72)	1996	312
Lower shoreline retreat rate (*m/yr*; -0.58)	2053	277
Upper age (*yrs*; 603)	2015	299
Lower Age (*yrs*; 573)	2028	290
Upper carbon inventory (*g C* m^{-2}; Interior= 7309.73; Edge= 5579.01)	2021	295
Lower carbon inventory (*g C* m^{-2}; Interior= 7205.73; Edge= 5475.01)	2022	294
Scarped		
Initial Simulation	1930	363
Upper shoreline retreat rate (*m/yr*; -0.88)	1903	397
Lower shoreline retreat rate (*m/yr*; -0.63)	1970	327
Upper age (*yrs*; 583)	1915	375
Lower age (*yrs*; 523)	1945	352
Upper carbon inventory (*g C* m^{-2}; Interior= 7163.25; Edge= 7303.15)	1930	363
Lower carbon inventory (*g C* m^{-2}; Interior= 7059.25; Edge= 7199.15)	1930	363

Outputs tabulated for model runs that utilized the upper and lower values for shoreline retreat, marsh age, and carbon inventory.

Figure 2.7: Net carbon budget and threshold width for Carrot Island Sites

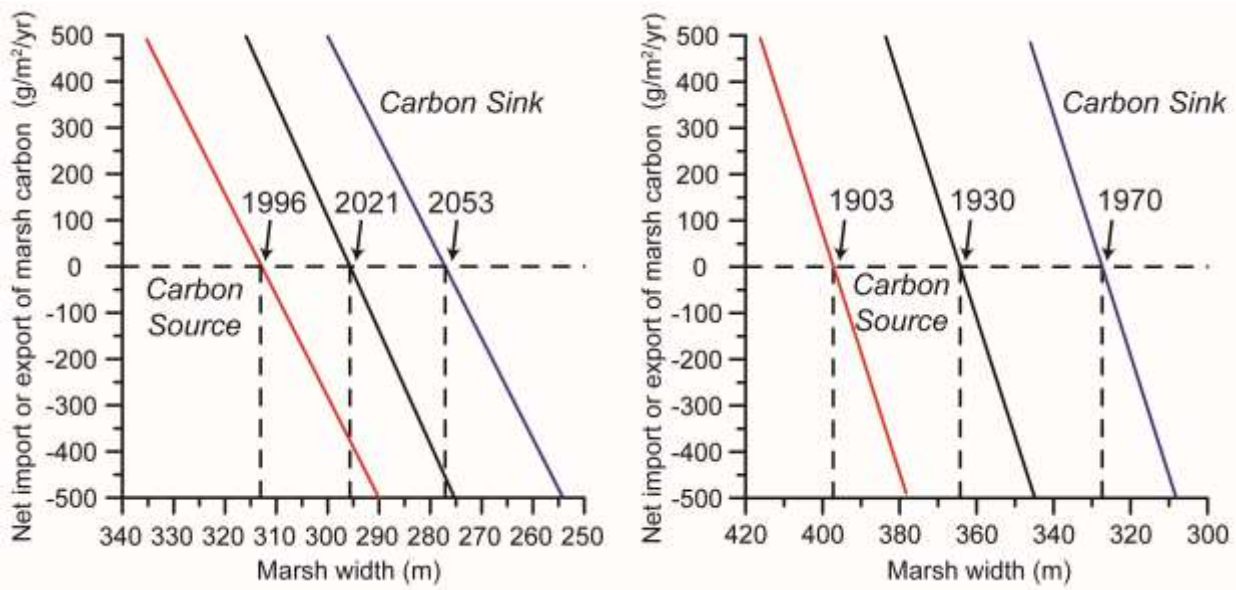

Net carbon budget and threshold width for both the ramped (left panel) and scarped (right panel) sections of Carrot Island. Black lines indicate the model output using the parameters measured from the vibracores and the decadal shoreline-retreat rate from the linear regression analysis of shoreline positions. The blue and red lines are the high and low estimates for the net carbon budget and threshold width determined by running the model with the high and low values for shoreline retreat rates. When the net carbon in the marsh is negative there is a net export of carbon into the estuary. The threshold width where the marsh becomes a carbon source is indicated for each model output with a vertical dashed line. (For interpretation of the references to color in this figure legend, the reader is referred to the web version of this article.)

2.4. Discussion

These simulations highlight the notion that although a fringing saltmarsh may be relatively wide and productive, it might not be functioning as a net carbon sink because of shoreline erosion. The uncertainties associated with the measurements used to parameterize the model have varied impacts on the threshold width. Errors in the marsh age and carbon inventory do not have a large effect on when the marsh transitions from a sink to a source because they are relatively low and change storage and export rates in the same direction (i.e. both are higher or lower; Table 2.2). In contrast, relatively small fluctuations in the retreat rate (~10 cm)

dramatically influence the timing and width when the marsh switches from sink to source because this impacts both the amount of carbon exported and the area available for carbon storage (Table 2.2). The rate of marsh erosion can fluctuate from year-to-year in response to storms, anthropogenic disturbances, or errors in measuring the retreat rate and these fluctuations will alter carbon export and storage. These results highlight the importance of accurately measuring marsh shoreline erosion as well as incorporating long term shoreline retreat rates in assessments of whether a marsh is a net carbon sink.

We tuned the model to Carrot Island using present-day (2013) rates of carbon storage and export and ran the model with the simplifying assumption that there were neither changes in carbon storage nor export rates in the past and future. Given that the model predicts the marsh along the more slowly eroding ramped site will switch to a source in less than 10 years, it is likely that this assumption is valid and that the rates of storage and export measured along this portion of Carrot Island will persist over this short time period. It is possible that carbon export and storage were different in the early 20th century when the more rapidly eroding scarped marsh reached the threshold width. However, given the large time span of data used to determine the retreat rates (1950s through 2012) and the consistent shoreline movement (high R^2 value of the linear regression; Figure 2.6) it is unlikely that carbon export was drastically different. Model users should consider whether erosion rates are likely to have changed through time, perhaps due to accelerated sea-level rise, subsidence, or anthropogenic influences, and parameterize the export term to reflect the rate change. The rate of carbon burial likely increased over the late 19th to early 20th centuries as the relative sea-level curve of Kemp et al. (2011) shows a three-fold increase in the rate of sea-level rise; however, it is unclear whether an increase in carbon burial

rate was associated with a concomitant increase in carbon decay at depth (Mudd et al., 2009; Kirwan and Blum, 2011; Kirwan and Mudd, 2012).

Although a fringing saltmarsh of any width is capturing carbon from the atmosphere and storing it, this box model takes a holistic view of the saltmarsh carbon budget by balancing the carbon storage term with shoreline erosion. Shoreline erosion is just one process of exchanging carbon between estuaries, the coastal ocean, and the atmosphere. Marsh carbon is a significant contributor to estuarine metabolism, which drives CO_2 release to the atmosphere (Cai, 2011; Canuel et al., 2012). The ultimate fate of the eroded saltmarsh carbon after it enters the estuary is uncertain (Bauer et al., 2013); however, it is clear that saltmarshes are a primary carbon-storage site and loss of marsh area will reduce the capacity of estuaries to store carbon (Canuel et al., 2012).

2.4.1. Model sensitivity

In our model, the threshold width is sensitive to changes in the rate of carbon storage, the rate of upland migration, and/or the rate of shoreline erosion, but not to changes in the carbon inventory (C). If C were half of what we measured in 2013, the threshold width and timing of the transition from source to sink would remain the same because C_s and C_e would be halved accordingly (Figure 2.8). Rates of carbon storage and export change as a function of sea-level rise and atmospheric temperature and the dynamics of these changes must be examined. Global warming and modest increases in the rates of sea-level rise (~5-10 mm yr^{-1}) are projected to lead to marsh transgression across the upland and increased rates of carbon burial (Mudd et al., 2009; Kirwan and Mudd, 2012; Morris et al., 2012), which could ultimately result in increased sequestration. This increase is contingent upon the marsh keeping pace with sea-level rise, such

Figure 2.8: Net carbon budget and threshold width at the ramped shoreline section of Carrot Island for scenarios of decreased carbon content, increased carbon storage rate, and decreased shoreline retreat rate

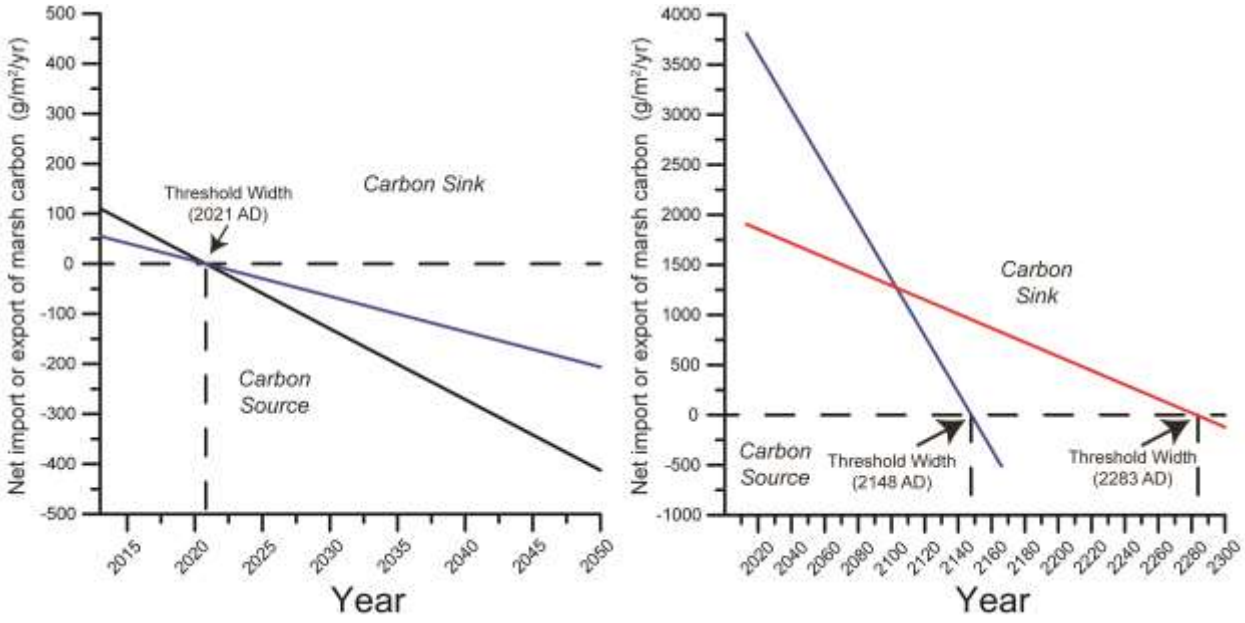

In the left panel the black line indicates the model output with the parameters from 2013 (same output as the black line in the left panel of Figure 2.7) and the blue line indicates the model output if the carbon content of the marsh was half of what was measured in the cores. In the right panel the red line indicates the model output if the shoreline retreat rate along the ramped section was half the decadal rate measured from 1958 to 2012 and the blue line indicates the output if the carbon storage rate were doubled after 2013. These scenarios suggest that reducing the shoreline retreat rate is the most effective way of preserving the carbon storage capacity of a saltmarsh.

that if a marsh drowns it will lose burial and sequestration capacity (Kirwan and Mudd, 2012). Increasing the carbon storage rate will increase the time it takes for a marsh to reach its threshold width (Figure 2.8); however, that increase in storage could be offset by an increase in export from shoreline erosion. Increased marsh shoreline erosion may result from sea-level rise (Mariotti et al., 2010), changes in storminess (Schwimmer, 2001), increase in the frequency and/or magnitude of wind waves or boat wakes (Houser, 2010), and impacts from adjacent shore-protection structures, such as sills (Mattheus et al., 2010). If sea-level rise changes the depth and fetch of the estuary, and/or if a greater volume of material is liberated from the marsh

via erosion because increased vertical growth has thickened the marsh (McLoughlin et al., 2015), carbon export may outpace any increase in carbon storage associated with sea level. The exact responses of marsh carbon storage and export to climate change are difficult to forecast and highly site dependent, thus these dynamics should be explored in a variety of geographic settings in order to further refine carbon budget models.

Reducing the shoreline retreat rate and/or increasing the storage rate are the most effective methods of extending the time it takes for a marsh to reach its threshold width and becoming a carbon source. Lower erosion rates reduce both the amount of carbon exported and the loss of marsh area available for carbon storage. For example, if the shoreline retreat rate were half the decadal rate we measured for the more slowly eroding ramped section of Carrot Island, then the marsh would remain a carbon sink until the year 2283 and the threshold width would narrow to 212 m (Figure 2.8). A similar outcome would occur if landward marsh migration balanced shoreline erosion; however, in many locations this is not likely due to steep upland topography or coastal development and the process of saltmarsh landward migration is slower than shoreline erosion, even in areas where upland gradients are low (Cahoon et al., 1998). If the carbon storage rate was doubled and the erosion rate held constant, then the marsh would remain a carbon sink until the year 2148 (threshold width of 212 m), not as long as halving the erosion rate. Reducing or stopping marsh shoreline erosion through the construction of sills, revetments, or oyster reefs will maintain marsh area and preserve the ability for a marsh to function as a carbon sink (Rodriguez et al., 2014); however, some of these modifications could have negative impacts to the quality of adjacent habitats (Needles et al., 2015).

2.5. Conclusions

Carbon export through shoreline erosion is commonly ignored in assessing the function of a saltmarsh as a carbon sink. Marshes that cannot transgress landward at a rate that balances shoreline erosion are narrowing and this impacts the capacity of the marsh to function as a carbon sink. Parameterized for a given saltmarsh, our model can be used to predict the threshold width where the marsh transitions from a carbon sink to a source based simply on changes in marsh area driven by shoreline erosion. Model simulations presented in this study highlight the importance of preserving existing marshes by slowing the shoreline-retreat rate in order to both maintain their ability to store carbon and to prevent the export of carbon to other coastal environments and ultimately the atmosphere. This is particularly pertinent in locations with low sediment supply as marshes are unlikely to naturally reestablish once lost (Kirwan and Megonigal, 2013). Although carbon storage rates could be greater in the future with global warming and future sea-level rise, that increase may not be enough to sustain marshes as carbon sinks if shoreline retreat rates remain the same or even increase. Coastal managers and conservationists can apply the model presented here to quantify the threshold width of other saltmarshes and evaluate the impact of modifications, like development, erosion mitigation, and restoration on the carbon budget. Additionally, if the goal of marsh restoration is carbon storage, then upland coastal development, erosion, and subsequent marsh narrowing must be considered to assess the success of these efforts.

CHAPTER 3: IMPACTS OF EROSION, OVERWASH, AND ANTHROPOGENIC DISTURBANCE ON THE CARBON BUDGETS AND CARBON RESERVOIRS OF TRANSGRESSIVE BARRIER ISLANDS

3.1. Introduction

3.1.1. Background

Changes in the areal extent of blue carbon habitats, such as saltmarshes, seagrass beds, and mangrove forests, impacts the global carbon budget, despite their small global footprint because these environments sequester and store carbon in their accreting sediments (Chmura et al., 2003; Murray et al. 2011). The high sedimentation rates in blue carbon habitats yields high carbon burial rates and an increase in the total amount of carbon stored in the soil (i.e. the carbon reservoir or stock) through time (McLeod et al., 2011; Chmura, 2013). Saltmarsh has the highest carbon burial rates of all the blue carbon habitats (~245 g C m^{-2} yr^{-1};Ouyang and Lee, 2014) and if a marsh is keeping pace with sea level and maintaining area the carbon reservoir will increase through time (Connor et al., 2001; Morris et al., 2012; Davis et al., 2015; Theuerkauf et al., 2016). Despite the important role saltmarshes play in the carbon cycle, their areal extent is decreasing globally, largely due to anthropogenic modifications to the coast (Duarte 2009; Nelleman et al 2009).

Saltmarshes are located in a variety of landscape settings, such as fringing the landward side of barrier islands, fringing the mainland along estuarine margins, in the middle of shallow lagoons, and river deltas (e.g. Godfrey and Godfrey, 1974; Susman and Heron Jr., 1979; Roberts, 1997; Mattheus et al., 2010; Rodriguez et al., 2013). Marsh carbon budgets have been explored in the context of climate change (Mudd et al., 2009; Kirwan and Mudd, 2012) and landscape

change (Theuerkauf et al., 2015); however, these models have not been applied to saltmarshes that fringe transgressive barrier islands (backbarrier fringing marshes). Backbarrier fringing marshes are included in global wetland inventories; however, the processes, such as erosion and overwash, associated with the landward movement of a transgressive barrier island complex during sea-level rise are not included in coastal carbon assessments.

Incorporating landscape change and marsh loss from shoreline erosion into carbon budgets of mainland fringing marshes has been shown to transition some sites from being a net carbon sink (increasing the carbon reservoir through time) to a net carbon source (decreasing the carbon reservoir through time; Theuerkauf et al., 2015). Building on that work, transgressive barrier island carbon budgets and reservoirs were explored in this study through the development and testing of a carbon budget model. This model includes carbon export from erosion at the ocean shoreface and backbarrier shoreline erosion as well as changes in carbon storage across the backbarrier marsh platform due to changes in marsh area resulting from backbarrier erosion and deposition of washover sediment during storms. Carbon budgets and the carbon reservoirs were examined at sites along two transgressive barrier islands that epitomize three different stages of transgression, including: 1. The early stage where the island is separated from the mainland by a large lagoon; 2. The middle stage where the island is separated from the mainland by a wide saltmarsh; and 3. The late stage, where the island is separated from the mainland by a narrow saltmarsh. The backbarrier marsh of the middle and late stage examples is characterized by tidal channels, a navigation channel and a mainland shoreline with a high gradient (~3% grade), which is not conducive to saltmarsh transgression. The aim of this work was to determine how storms, changes in the rate of shoreline erosion, and geologic setting have impacted barrier island

carbon budgets and reservoirs across the last century using empirical data, and apply results to explore the future of barrier island carbon storage.

3.1.2. Conceptual model of carbon storage and export in transgressive barrier islands

Substrate for backbarrier marsh colonization is primarily created during transgression through deposition of flood tidal deltas and washovers (Godfrey and Godfrey, 1974). Both of these deposits are associated with and commonly form at low-elevation narrow parts of barrier islands (Leatherman, 1979; Donnelly et al., 2006). Washover deposits form during storms when the ocean overtops the barrier, transporting beach and shoreface sand across the island where it is deposited in the lagoon or estuary (Donnelly et al., 2006; Lorenzo-Trueba and Ashton, 2014). Flood tidal deltas form during storms as strong currents erode a channel through the island, which is a conduit for flood-tide transport of beach- and shoreface-sand to the lagoon or estuary where it is deposited as delta lobes (Leatherman, 1979). Washover and tidal inlet deposition builds island width and helps to sustain transgressive barrier islands through time by balancing the loss of area from ocean and backbarrier shoreline erosion (Leatherman, 1983; Timmons et al., 2010).

After the storm, island overwash stops or the tidal inlet fills in and intertidal portions of the washover and flood-tidal delta deposits are often colonized by saltmarsh grasses. Marsh colonization likely occurs rapidly once the substrate reaches an intertidal elevation and conditions are optimal for marsh growth. At this point, the carbon reservoir of the barrier island increases rapidly as the once bare backbarrier sediments become a carbon sink. After these backbarrier marshes are established, they grow vertically to keep pace with sea-level rise through organic and inorganic deposition (Redfield, 1962; Nyman et al., 2006). Overwash and aeolian-transported sand provide an important source of inorganic sediment for vertical marsh growth

(de Groot et al., 2011; Rodriguez et al., 2013). Organic deposition occurs during the life cycle of marsh grass (autogenic process) as well as by trapping of allogenic organic material from both terrestrial and other aquatic sources (Ember et al., 1987). Marshes sequester carbon by removing CO_2 from the atmosphere and storing it in both aboveground and belowground biomass (IPCC 2014). This sequestered carbon accumulates in marsh sediments and the fraction of carbon that remains in the soil over longer time scales (decades to millennia) after microbial degradation is considered to be buried. Carbon storage is the carbon inventory of the marsh (total carbon of the marsh sediment within a specified sample area) integrated across the lifetime of the marsh (i.e. from the marsh surface to its base). The depositional processes of marsh soil formation results in an increase in the amount of carbon contained within the entire marsh site, which is referred to in this study as the carbon reservoir.

Transgressive barrier islands may represent an important global carbon sink since the carbon reservoir will increase through time if backbarrier marshes keep pace with sea-level rise and maintain their area. Additionally, the formation of washover fans and flood tidal deltas may expand marsh area and increase the barrier island carbon reservoir. However, carbon export from shoreline erosion must also be included in the barrier island carbon budget and if export exceeds burial, the barrier could function as a source of carbon. Carbon is exported from backbarrier marsh shoreline erosion and ocean shoreline erosion as a transgressive barrier island migrates landward in response to sea-level rise, a process known as barrier rollover. During barrier rollover, backbarrier marsh sediments are buried by washover, dune, and/or beach deposits before they are eventually exposed on the shoreface and eroded. Backbarrier marshes also experience erosion from estuarine waves and currents that are generated from human disturbances, winds, and storm events (Riggs and Ames, 2003; Elliott et al., 2015). The erosion

of organic-rich marsh deposits will export carbon from the barrier-island system, to the coastal ocean and estuary; however, the lability and ultimate fate of the carbon will dictate what proportion is released back into the atmosphere (Cai et al., 2003; Canuel et al., 2012). The net carbon budget of a transgressive barrier island over any time scale is the difference between the amount of carbon stored across the marsh platform and the amount of carbon exported from shoreface erosion and backbarrier shoreline erosion (Figure 3.1). The trajectory of the carbon budget will dictate the trajectory of the barrier island carbon reservoir through time. For example, if carbon storage exceeds export the barrier island will function as a carbon sink and the reservoir will increase through time. Changes in storminess, sea-level rise, land-use, and coastal management influence rates of erosion and the areal distribution of saltmarsh, which could alter the carbon budget and reservoir of a barrier island by changing carbon export and burial rates.

Figure 3.1. Conceptual model of the transgressive barrier island carbon budget

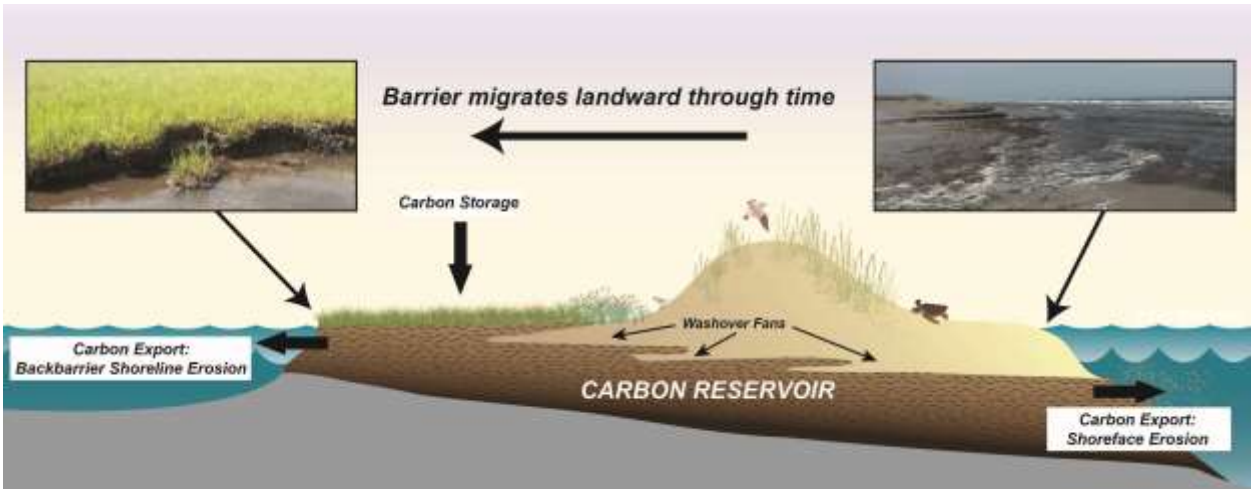

Left top panel depicts an eroding backbarrier marsh shoreline and the right top panel depicts old marsh deposits outcropping and eroding on the shoreface.

3.2. Methods

3.2.1. Study sites

Carbon budgets were developed for sites along Onslow Beach and Core Banks, two transgressive barrier islands in Eastern North Carolina, U.S.A. (Figure 3.2). Core Banks is an undeveloped transgressive barrier island located within the Cape Lookout National Seashore. The island is characterized by expansive backbarrier marshes (maximum width ~1.8 km) that extend into a ~3-4.5 km-wide open-water lagoon (Core Sound), eroding oceanfront and backbarrier shorelines, and a barrier lithosome composed primarily of beach, relict inlet, and washover sediments (Moslow and Heron 1978; Moslow and Heron, 1981; Heron et al., 1984; Figure 3.2). Numerous ephemeral tidal inlets punctuated Core Banks during the late-Holocene transgression (Moslow and Heron, 1981; Mallinson et al., 2008). Great Island, the site of a former tidal inlet (Heron et al., 1984), was selected as the study area along Core Banks (Figure 3.2). At this site, the distance from the ocean shoreline to the backbarrier marsh is ~200 m, the backbarrier marsh is ~1,200 m-wide, and the North Carolina Division of Coastal Management (NCDCM) shoreline change data indicates that from 1979-2011 the beach is currently eroding at a rate of around 1.5 m/yr.

Figure 3.2. Chapter 3 study area map: Core Banks and Onslow Beach, NC

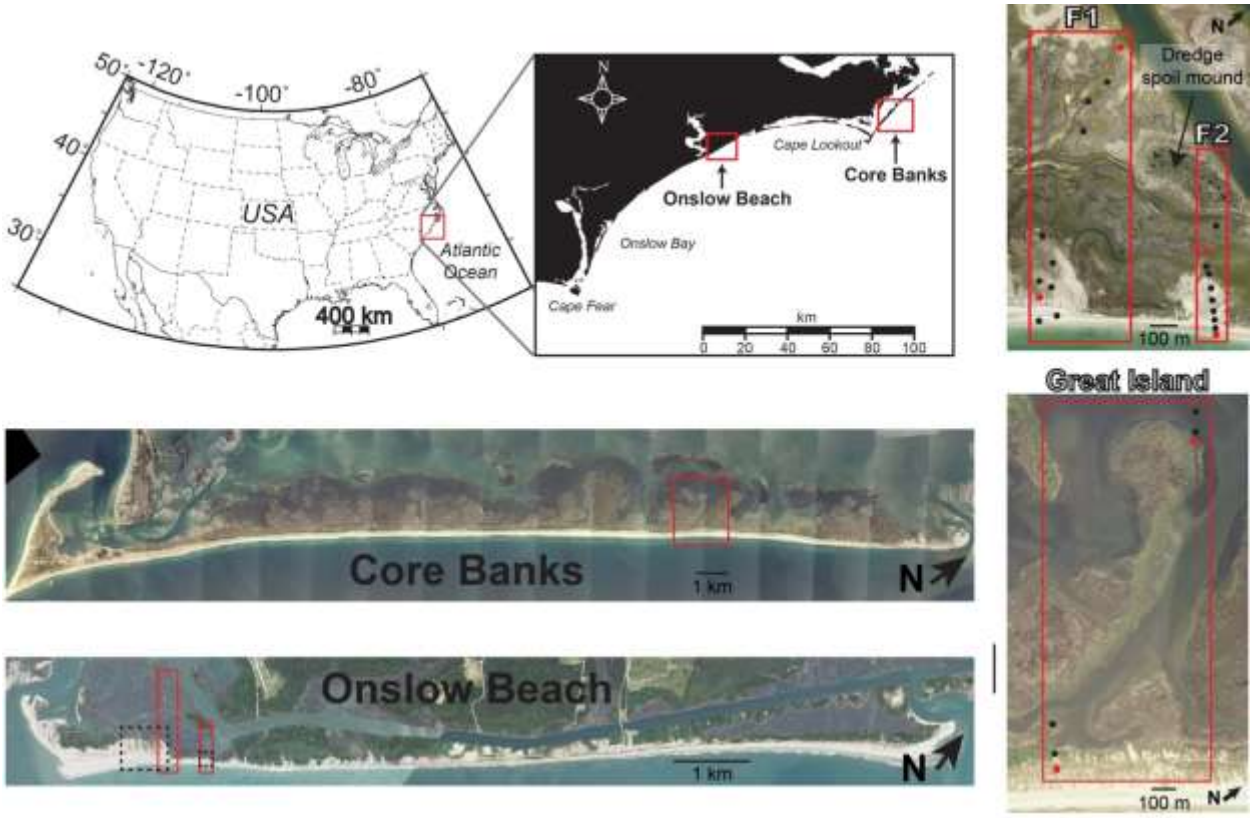

(Top left) Regional study area map depicting the locations of Core Banks and Onslow Beach. (Center) Core Banks aerial photograph with red box denoting the Great Island study area. (Bottom left) Onslow Beach aerial photograph with red boxes denoting the F1 and F2 study sites (red boxes). Dashed boxes indicate the location of photos used in Figure 7. (Right) Vibracore locations at the Onslow Beach (top right) and Great Island (bottom right) sites, respectively. Red dots indicate cores sampled for percent organic carbon and radiocarbon analyses. All aerial photographs provided by the United States Department of Agriculture (USDA).

Onslow Beach is a transgressive barrier located ~75 km southwest of Core Banks (Figure 3.2). The island is part of Marine Corps Base Camp Lejeune; thus, portions of the island are utilized for military training and recreation. The northern and southern portions of the island remain undeveloped, while the middle stretch of the beach contains light development, such as access roads and small recreational cabins, but no permanent human residents (Figure 3.2). In contrast to Core Banks, Onslow Beach lacks an open water lagoon on its landward-side. During

the late-Holocene when the island was farther offshore, an open-water lagoon did exist behind Onslow Beach; however, rapid transgression migrated the island to its current position (Yu, 2012), where it is only separated from the mainland by backbarrier marsh (maximum width ~1 km) and a navigational channel, the Intracoastal Waterway (ICW). Historically, the position of the ocean shoreline along the northeastern end of the island has been relatively stable, while the ocean shoreline along the southwestern end of the island is experiencing rapid rates of erosion and transgression (2-4 m/yr; Benton et al., 2004; Theuerkauf and Rodriguez, 2014). The southwestern portion of the island is characterized by low elevation dunes (<2 m), narrow beach widths (~100 m), and frequent overwash during storms (VanDusen et al., 2016).

Two study sites, F1 and F2, were selected that exemplify the morphology of this portion of Onslow Beach. Over the past century, both of these sites have been characterized by low barrier elevations, a history of ocean overwash during storms, and ocean shoreline erosion and transgression (Yu, 2012). Within the past 20 years, four hurricanes have altered the morphology of these two sites. In September of 1996, Hurricane Fran formed a large washover terrace at F1, which subsequently increased in landward extent during Hurricane Bonnie in August of 1998. Hurricane Irene, which made landfall near Cape Lookout, NC in August 2011 created a washover terrace at F2. This terrace was subsequently modified into a washover fan during Hurricane Sandy in October 2012 and frequent nor'easters during the winter of 2012-2013 (Van Dusen et al., 2016).

3.2.2. Data collection

To model changes in the net carbon budget at each of the sites carbon storage and export must be calculated. The rate of carbon storage (g yr^{-1}), can be estimated from measuring saltmarsh sedimentation rates, sediment composition, and changes in marsh area. Saltmarsh

sediment thickness and composition and rates of backbarrier erosion and/or beach erosion are used to estimate the rate of carbon export (g yr^{-1}). Field measurements taken at specific sites are likely not representative of the entire barrier island; however, given that the aim of this study was to examine changes to carbon budgets through time we collected data and apply the carbon model at specific sites, rather than examining along-barrier variations in carbon storage. Budgets were computed along shore-perpendicular transects that are 1-m wide in the along-beach direction. The model was parameterized with information from vibracores and a time-series of aerial photographs.

3.2.2.1. Vibracores

Vibracores were collected along shore-normal transects at each of the three study sites from the ocean shoreline landward to either the backbarrier lagoon or the ICW (Figure 3.2). Survey data (horizontal and vertical position) were gathered with a Trimble Real-Time Kinematic-Global Positioning System (RTK-GPS) at each core location as well as along a profile at each coring transect.

Cores were transported to the University of North Carolina at Chapel Hill Institute of Marine Sciences where they were split along their long axis, photographed, described, and sampled to define sedimentary facies and determine the carbon inventory and age of marsh units. Carbonaceous units were subsampled in continuous 5-cm increments from one half of the split cores for organic carbon analysis. Samples were dried and homogenized with a grinder and a mortar and pestle. A Costech ECS4010 Elemental Analyzer was used to measure percent organic carbon on subsamples of the carbonaceous sediment and values were reported with a ±0.17% error (Theuerkauf et al., 2015). Percent organic carbon was transformed into grams of carbon/m^2 based on the mass of the sample and the area of the core (45.6 cm^2). To determine

when saltmarsh first colonized the area, aboveground biomass (e.g. grass blades, stems, and seeds) was sampled from the base of the marsh units and sent to Beta Analytic for carbon-14 dating. This technique assumes that the material dated was preserved *in situ* (Redfield and Rubin, 1962). Radiocarbon dates were calibrated using IntCal13 (Reimer et al., 2013).

3.2.2.2. Changes in shoreline position and marsh area

Backbarrier and oceanfront shoreline erosion rates were measured using United States Department of Agriculture (USDA) aerial photographs, digitized shorelines downloaded from the NCDCM, and terrestrial laser scanning data. Erosion rates were developed using the ArcGIS extension Digital Shoreline Analysis System (DSAS) (Thieler et al., 2009). DSAS calculates the distance each shoreline is from a baseline along specified transects. Rates of shoreline erosion were calculated for each time step using the end-point method to explore the effects of changing shoreline erosion rates on the annual carbon budget.

Ocean shoreline retreat rates over decadal to centennial time scales were developed at Core Banks and Onslow Beach using publically available shorelines digitized from a combination of T-sheets and aerial photographs, which have vertical resolutions ranging from 1.5-10.8 m. The dates of the ocean shorelines used for Core Banks were 1866, 1988, 1998, 2004, and 2014 and the dates used for Onslow Beach were 1872, 1934, 1997, and 2004. Ocean shoreline retreat rates over yearly time scales for the Onslow Beach sites were measured during biannual surveys from 2007 to 2014 using a terrestrial laser scanner (Theuerkauf and Rodriguez, 2014). These data capture shoreline changes associated with extensive washover deposition during Hurricanes Fran, Bonnie, Irene and Sandy. The shoreline position was extracted from digital elevation models constructed using topographic data from the laser scans. Along Onslow Beach, the shoreline is approximated by the mean high water line, which is defined as the 0.36 m

NAVD88 contour (Weber et al., 2005). At Great Island, ocean shoreline retreat rates over yearly time scales were not derived because based on visual inspection of the 2004 and 2014 aerial photographs, there appeared to be no obvious morphologic impacts from hurricanes strikes since 1998. Backbarrier shorelines at Core Banks and Onslow Beach were digitized for this study from USDA aerial photographs using ArcGIS. At Onslow Beach aerial photographs from 2009, 2010, 2012, and 2014 were used to calculated backbarrier shoreline retreat rates. At Core Banks aerial photographs from 2009, 2010, 2012, and 2014 were used to calculated backbarrier shoreline retreat rates.

Aerial photographs were used to measure long-term changes in marsh area from backbarrier erosion and to measure recent changes in marsh area related to burial and erosion from storms and dredging of the ICW. The initial marsh width was measured from the earliest available map for each site; AD 1866 for Core Banks and AD 1872 for Onslow Beach. Marsh area was then computed as marsh width multiplied by the 1-m length of marsh shoreline examined in this study. Change in marsh area through time was determined using backbarrier shoreline erosion rates and measurements from aerial photographs of marsh loss in response to ICW dredging and washover deposition. The carbon budget model does not include fragmentation of the marsh through time from sea-level rise and expansion of the tidal creek network, thus the only way marsh can be lost in the model is through burial by overwash or removal by erosion and dredging.

3.2.3. Carbon budget and reservoir

The first known position of the ocean shoreline at Core Banks and Onslow Beach, AD 1866 and AD 1872, respectively, was used as the starting point for the model, which is run forward in time to the present. Carbon storage was parameterized through a combination of data

from the coring surveys and aerial photographs (Figure 3.2; Table 1). Total carbon storage (g/yr) is the product of the rate of carbon accumulation (g m^{-2} yr^{-1}) in the backbarrier marsh and the area of the marsh (m^2). The rate of carbon accumulation was estimated by dividing the carbon inventory (g m^{-2}) by the age of the marsh (yr) determined from the radiocarbon date collected at the base of the marsh. Shoreface carbon export (g yr^{-1}) is the product of the shoreface carbon inventory (g m^{-2}), measured using one core on the shoreface at each transect (Figure 3.2), the shoreface erosion rate (m yr^{-1}), and the length of the shoreline (m). Backbarrier carbon export (g yr^{-1}) is the product of the marsh carbon inventory (g m^{-2}), the rate of backbarrier marsh shoreline erosion (m yr^{-1}), and the length of the shoreline (m). The marsh carbon inventory for carbon export was computed using the same cores as carbon storage.

The initial carbon reservoir (g) was calculated as the product of the total carbon inventory (g m^{-2}) for the entire cross-section at each site (marsh inventory + shoreface inventory) and the estimated area across each site for the first year of the model (m^2; backbarrier marsh area + beach area). For each subsequent year, the calculated net carbon budget was either added or subtracted from the reservoir. The carbon reservoir was computed every year from AD 1866 (Core Banks) and AD 1872 (Onslow Beach) to 2014 at each study site.

3.3. Results and Interpretations

3.3.1. Sedimentology and stratigraphy

3.3.1.1 Core Banks

Heron et al (1984) and Moslow and Heron (1978) identified the Great Island section of the barrier as a relict flood tidal delta based on a series of cores collected along the length of Core Banks. Those cores revealed a typical transgressive barrier sequence with modern beach and dune units perched on top of older washover and saltmarsh units. Old tidal inlets were

identified as thick coarse-grained units mapped as being discontinuous in an along-beach direction. Those inlet-fill deposits were always sampled adjacent to relic flood-tidal deltas preserved in Core Sound, like Great Island. The cores collected in this study sampled those same previously identified units.

The deepest unit (-0.4 to -2.8 m NAVD88) sampled in the Great Island cores collected for this study, was a medium to coarse sand unit with multiple shell hash beds and <1% organic carbon (Figure 3.3). In some cores, this unit manifested as a coarsening upward sequence capped by a shell hash deposit. We interpreted this facies as the tidal inlet environment.

Saltmarsh was sampled as a carbonaceous (0.2 to 9% organic carbon) dark greenish-gray silt unit with abundant plant material that averages 32.5 cm ±14.8 cm in thickness (Figure 3.3). Saltmarsh was sampled continuously across the island, is located at the top of cores collected in the modern backbarrier marsh, and is directly above the tidal inlet complex. The carbon content of this unit was highest in the samples collected within the modern backbarrier marsh (~3-9%),which show increasing percent organic carbon with depth to ~ 20 cm, below that depth percent organic carbon decreases. In the most seaward core collected on the beach, the marsh

Figure 3.3. Stratigraphic cross-section of Great Island, Core Banks, NC

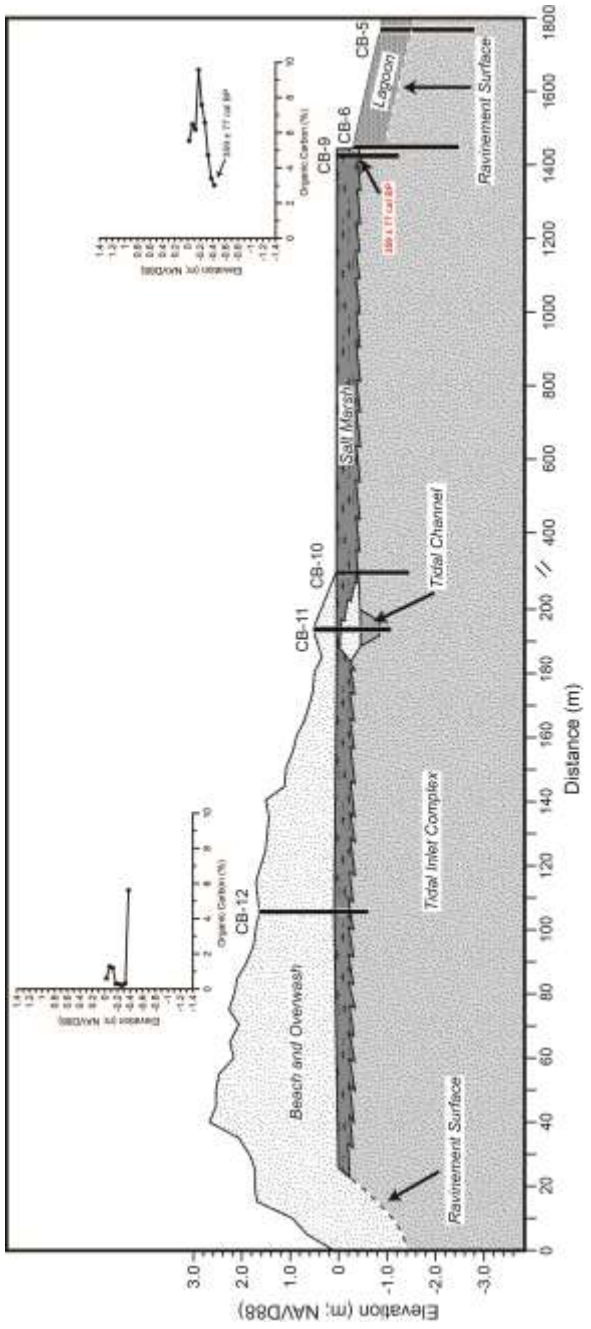

CHN profiles measured from cores CB-12 and CB-9 are also shown. More information on the radiocarbon dates can be found in Appendix 3.1.

unit had a lower percent organic carbon (0.2% to 5.6%) than what was sampled in the modern backbarrier marsh. The general trend in this core was higher percent organic carbon values in the upper 15 cm with decreasing percentages moving down core. Directly behind and on the modern beach, the marsh unit is buried by medium to coarse grained sand of washover, dune and/or beach deposits. A radiocarbon date at the base of the marsh unit indicated that the marsh first colonized the area 359 ±77 cal BP. Cores collected on the modern bay bottom of Core Sound did not sample any marsh material, suggesting that as the back-barrier shoreline recedes no marsh material is preserved.

3.3.1.2. Onslow Beach

Cores collected at F1 and F2 sampled the same transgressive barrier sequence as Yu (2012) identified at Onslow Beach. The general sequence at both sites was a basal Pre-Holocene unit overlain successively by lagoonal, saltmarsh, washover, beach and dune deposits (Figure 3.4). The Pre-Holocene unit ranged in character from stiff clay to fine-grained sand and is indicative of subaerial exposure during a period of lower sea-level (Yu, 2012). The lagoonal unit was sampled as a muddy sand with silty laminae, that ranged in thickness from 0.2 m to 2.0 m, contains <1% organic carbon, and was radiocarbon dated to ~1000 cal BP (Yu, 2012).

Washover deposits at F1 that formed during Hurricanes Fran (1996) and Bonnie (1998) and at F2 that formed during Hurricanes Irene (2011) and Sandy (2012) were sampled in our cores immediately seaward of the modern backbarrier marsh (Figure 3.4). At F1, this facies was characterized by stacked fining upward sequences of gravelly-coarse sand to medium-grained sand with heavy mineral laminae. At F2, the washover unit is medium-to-coarse sand with abundant shell hash, gravel, and heavy mineral laminae. The seaward cores at F1 sampled

Figure 3.4. Stratigraphic cross-sections for Sites F1 and F2, Onslow Beach, NC

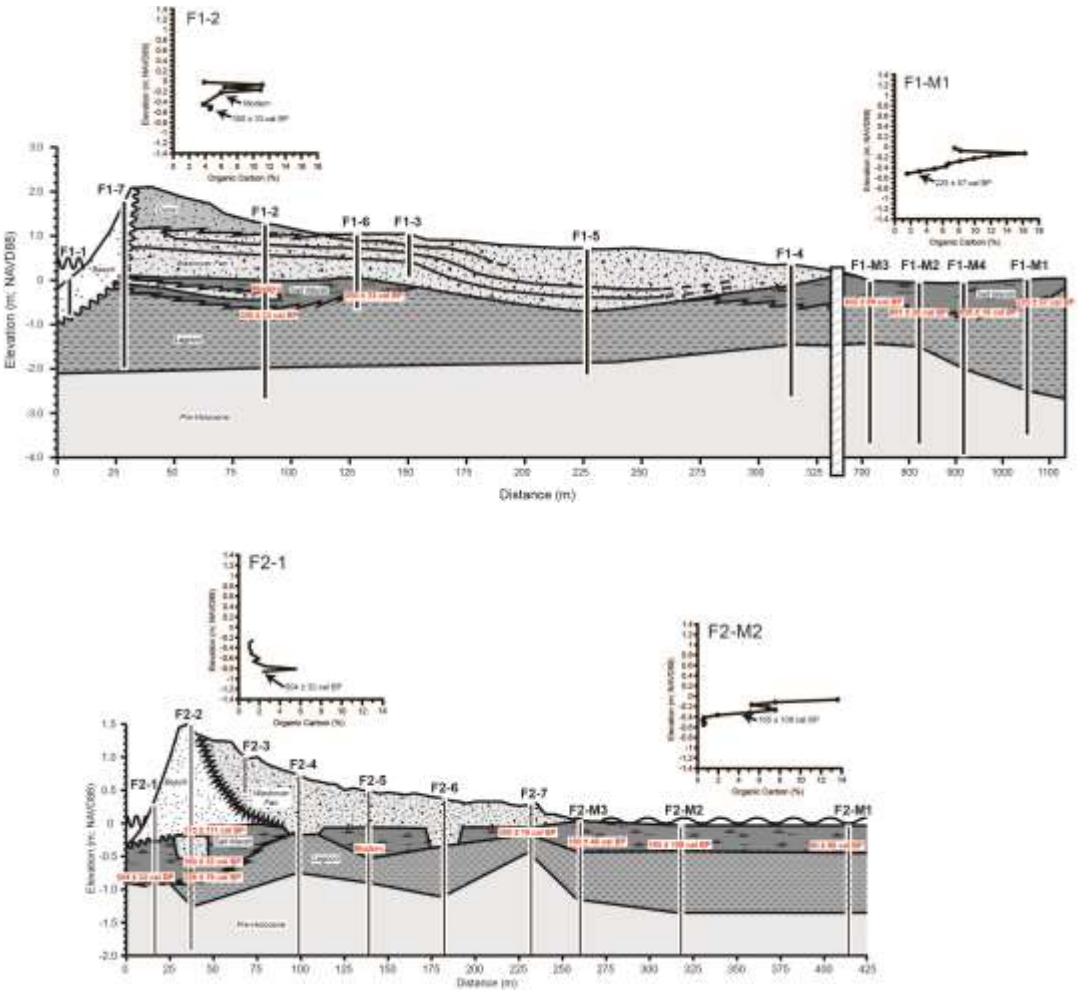

CHN profiles measured from shoreface cores F1-2 and F2-1 as well as backbarrier marsh cores F1-M1 and F2-M2 are shown. More information on radiocarbon dates can be found in Appendix 3.1.

modern beach and dune sand perched above the lagoonal unit and organic-rich saltmarsh sediment. Only saltmarsh sediment was sampled below the beach sand at Site F2, due to the shallow depth of the pre-Holocene unit, which limited accommodation at that location during Holocene sea-level rise (Yu, 2012). .

The backbarrier marsh was sampled at both sites as an olive gray to brownish gray carbonaceous muddy sand to sandy silt unit with abundant plant material and extends seaward

underneath the dunes and washover deposits (Figure 3.4). Cores collected in the modern marsh at F1, sampled saltmarsh ranging in thickness from 60 to 80 cm in direct contact with the lagoonal unit. Percent organic carbon ranges from 1 to 11% in these cores and reaches a maximum around 15 cm down core. Vegetation sampled from the base of the backbarrier marsh unit and radiocarbon dated indicate that the marsh colonized the area between 225 ± 57 cal BP and 681 ± 28 cal BP. The marsh unit sampled in the beach cores at F1 is thinner and interfingered with washover sand. Vegetation from the base of the marsh unit here was radiocarbon dated as 300 ± 33 cal BP. Percent organic carbon of the marsh sediment sampled below the beach sand ranges from 4 to 11% with the highest values in the marsh unit below the washover sand beds. The modern backbarrier saltmarsh at F2 ranges in thickness from 20 to 50 cm and based on radiocarbon dates from the base of the unit, in age from 80 ± 68 cal BP to 300 ± 19 cal BP. Percent organic carbon of the backbarrier saltmarsh sediment ranges from ~1 to 13% with a maximum at the top of the core and decreasing percent carbon down core. Around 60 cm of older marsh material was sampled below sand in cores collected on the beach. A radiocarbon date at the base of this unit yielded an age of 504 ± 32 cal BP and percent organic carbon ranges from 1 to 6% with a maximum near the bottom of the unit.

3.3.2. Changes in erosion rates and marsh area

Rates of ocean shoreline erosion at Great Island were nearly constant from the late 1800s to the early 1990s. Since the 1990's rates of ocean shoreline erosion have varied; which is likely due to increased fidelity of the aerial photographic record and storm impacts during the recent past (Figure 3.5; Table 1). The ocean shoreline migrated ~30 m landward at Great Island from 1866 to 2014, with most of the erosion occurring from 1988 to 2004. At Onslow Beach, from 1872 to 2014 the ocean shoreline at F1 and F2 moved landward ~255 m and ~200 m,

respectively. From AD 1872 to 1995, both Onslow Beach sites were either stable or slowly eroding (Figure 3.6; Table 1). Since 1995, the rates and directions of change have fluctuated, and similar to Core Banks, this short-term variability is due to storm impacts captured by the increased frequency of recent aerial photography (Figure 3.6). Site F1 oscillated between accretion and erosion after the 1934-1995 time-step and since 2007 the shoreline has been prograding seaward. This accretion is likely related to post-storm recovery after Hurricane Fran. At F2, the rate of shoreline change increased across the 20th century, but has remained relatively constant throughout the 20th century with the exception of storm events (Figure 3.6).

Since marsh erosion rates were calculated with recent data (since 2009) no inferences can be made about changes in the rates through time. The marsh shoreline at Great Island is eroding around 0.25 m per year. At Onslow Beach, the marsh shoreline at F1 is eroding ~0.25 m/yr. The marsh shoreline is not eroding at F2 because when the ICW was constructed, dredged material was placed on top of the marsh adjacent to the ICW forming a ~1.5- m-high sand mound that has since been colonized by maritime forest and buffers the marsh shoreline from erosion.

Marsh area has been decreasing at the Core Banks and Onslow Beach sites since the 1800s. At Great Island, backbarrier shoreline erosion is assumed to have driven marsh area loss (Figure 3.5). Rates of marsh loss have varied through time at both Onslow Beach sites (Figure 3.6). Marsh narrowing due to backbarrier erosion is a relatively continuous process; however, storms and human disturbances can result in large, abrupt marsh loss, such as the instantaneous reduction in marsh width at Onslow Beach with the construction of the ICW in 1932 (Figure 3.6). F1 lost around 460 m^2 of marsh during the construction of the ICW, while F1 lost around 130 m^2. In 1996, overwash from Hurricane Fran abruptly buried 180 m^2 of the marsh at F1 (Figures 3.6 and 3.7). Two years later, 110 m^2 of marsh at F1 was buried by Hurricane Bonnie.

In 2011, around 30 m^2 of marsh was rapidly buried at F2 during Hurricane Irene (Figures 3.6 and 3.7). In the following year, around 150 m^2 of marsh was buried at F2 during Hurricane Sandy and subsequent nor'easters (Figure 3.6 and 3.7; Van Dusen et al., 2016).

Table 3.1. Parameters used in the transgressive barrier island carbon budget models

Ocean Shoreline Erosion Rate (m/yr)	
Great Island 1866-1988	-0.00275
Great Island 1988-1998	-0.43575
Great Island 1998-2004	-3.0765
Great Island 2004-2014	-0.7115
Onslow Beach F1 1872-1934	-1.25
Onslow Beach F1 1934-1995	-1.066
Onslow Beach F1 1996 (Hurricane Fran)	-7.272
Onslow Beach F1 1997-2004	0.166
Onslow Beach F1 2004-2007	-3.6
Onslow Beach F1 2007-2014	2.88
Onslow Beach F2 1872-1934	0.09
Onslow Beach F2 1934-1995	-1.106
Onslow Beach F2 1996 (Hurricane Fran)	-5.162
Onslow Beach F2 1997-2004	-5.3
Onslow Beach F2 2004-2007	-3.136
Onslow Beach F2 2007-2010	-0.77
Onslow Beach F2 2011	-10.14
Onslow Beach F2 2012	-7.5
Onslow Beach F2 2013-2014	-0.77
Backbarrier Shoreline Erosion Rates(m/yr)	
Great Island	-0.25
Onslow Beach F1	-0.25
Onslow Beach F2	0
Carbon Inventory (g C m^{-2})	
Great Island Marsh (CB-9)	8891.93
Great Island Shoreface (CB-12)	3949.71

Onslow Beach F1 Marsh (F1-M1)	10423.10317
Onslow Beach F1 Shoreface (F1-2)	13393.96
Onslow Beach F2 Marsh (F2-M2)	9913.78
Onslow Beach F2 Shoreface (F2-1)	10388.18

Marsh Age (yrs)	
Great Island (CB-9)	423.00
Onslow Beach F1 (F1-M1)	288
Onslow Beach F2 (F2-M2)	228

Marsh Carbon Accumulation Rate (g C m^{-2} yr^{-1})	
Great Island	21.02112073
Onslow Beach F1	36.19133046
Onslow Beach F2	43.48149123

Figure 3.5. Great Island shoreface erosion rates and marsh area change

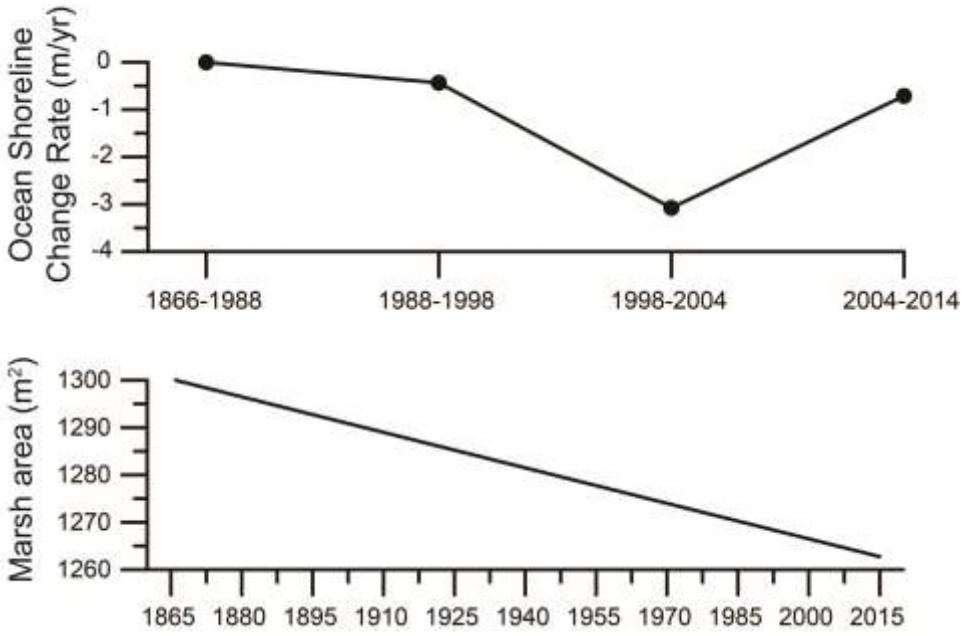

(Top) Ocean shoreline erosion rates from 1866 to present. (Bottom) Marsh area through time depicting a gradually narrowing marsh over the last century.

Figure 3.6. Onslow Beach shoreface erosion rates and marsh area change

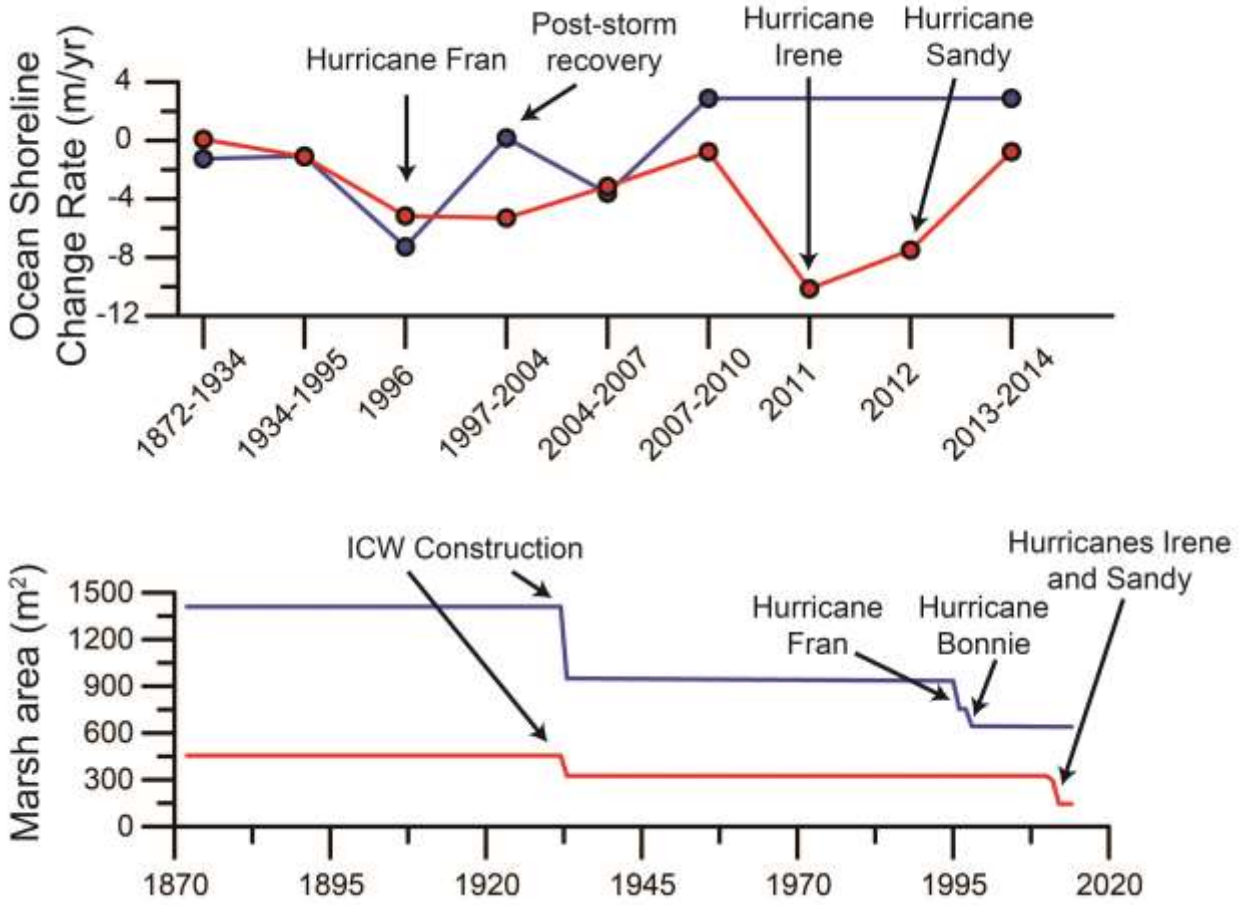

Site F1 shown in blue and Site F2 shown in red. (Top) Ocean shoreline erosion rates through time at both sites. (Bottom) Marsh area through time at the Onslow Beach sites. Major erosional and depositional events are annotated on the graphs.

Figure 3.7. Graphical depiction of the impact of overwash on marsh area

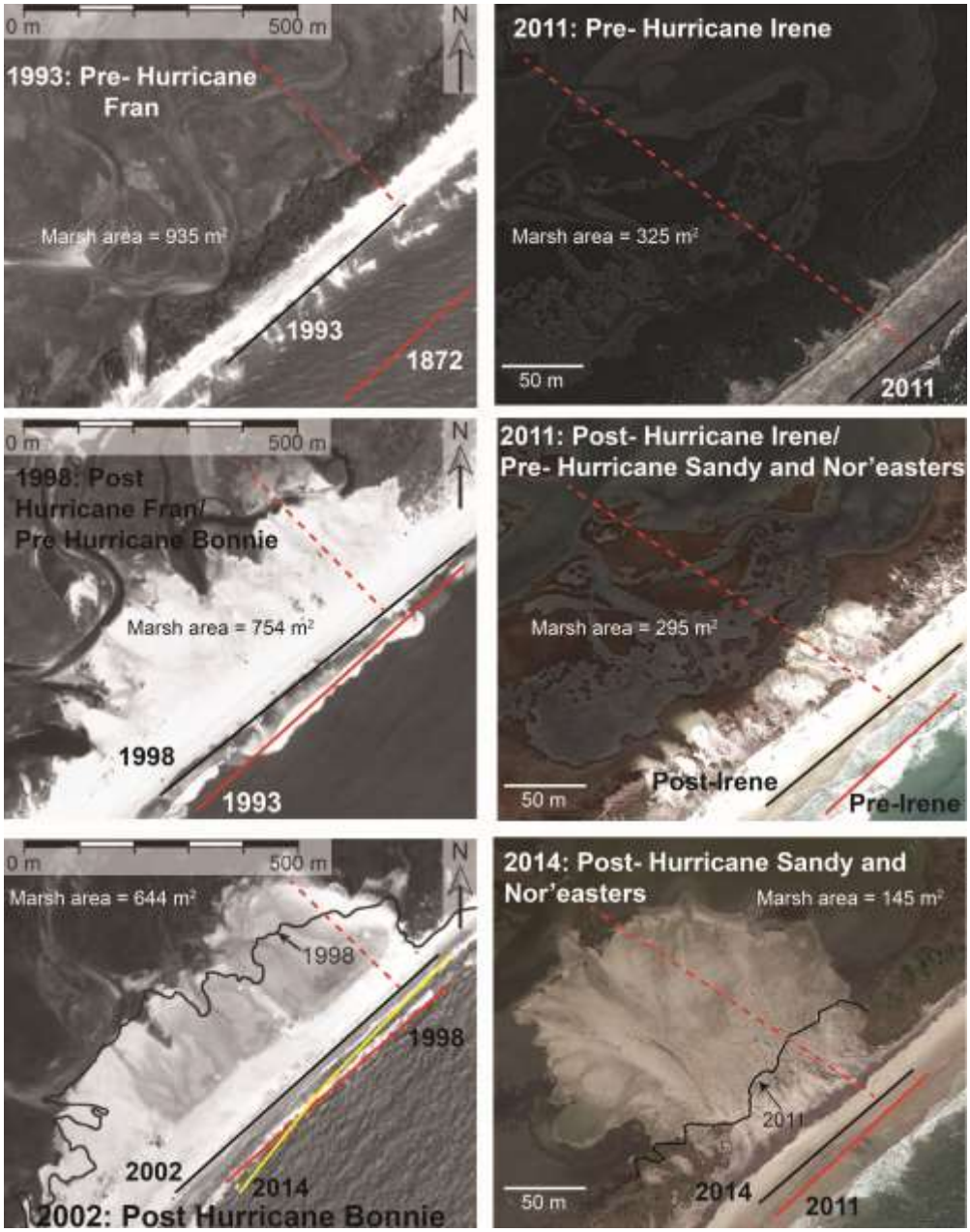

Onslow Beach Site F1 (left) experienced marsh loss during Hurricanes Fran and Bonnie and Site F2 (right) experienced marsh loss during Hurricanes Irene and Sandy. The transect used for the carbon budget model is denoted in each photograph with a dashed red line. Shorelines used in the erosion rate calculations are denoted with solid red, black, and yellow lines. Marsh area is annotated on each figure. The landward extent of the Hurricane Fran washover deposit is denoted by a solid black line on the 2002 photograph and the landward extent of the Hurricane Irene washover deposit is annotated by a solid black line on the 2014 photograph.

3.3.3. Carbon budget model

3.3.3.1 Core Banks

The core data combined with shoreline erosion and marsh areal change data were used to develop the carbon storage and export rates (Figures 3.8 and 3.9; Table 1). At Great Island, carbon accumulation rates were 21.02 g C m^{-2} yr^{-1}. This rate is based on a carbon inventory of 8891.9 ±15.1 g C m^{-2} (core CB-9) and a marsh age of 359 ±77 cal BP. Total carbon storage decreases slightly through time as the marsh narrows in response to backbarrier shoreline erosion (Figure 8). Carbon export rates at Great Island vary through time with shoreface erosion rates, since the shoreface carbon inventory, which was 3949.7 ± 6.7 g C m^{-2} (core CB-12) and backbarrier shoreline erosion rates are constant through time (Figure 8).

The net carbon budget at Great Island is always positive, thus this portion of Core Banks always functioned as a carbon sink (Figure 3.8). However, the net budget does fluctuate through time because of variations in the rate of carbon export related to changes in the rate of ocean shoreline erosion. The carbon reservoir at Great Island has steadily increased throughout the past century; however, the rate is less during years when the net budget is lower (Figure 3.8).

3.3.3.2. Onslow Beach

Carbon storage and export rates vary more through time at Onslow Beach than at Core Banks (Figure 3.9). At F1, the marsh carbon accumulation rate is 36.19 g C m^{-2} yr^{-1}, which is based on a carbon inventory of 10423 ±17.7 g C m^{-2} and an age of 225 ±57 cal BP (core F1-M1). The marsh carbon burial rate at F2 is 43.48 g C m^{-2} yr^{-1}, which results from a carbon inventory of 9913.78 ±16.9 g C m^{-2} and an age of 165 ± 108 cal BP (core F2-M2). Sudden

Figure 3.8. Great Island carbon budget and carbon reservoir

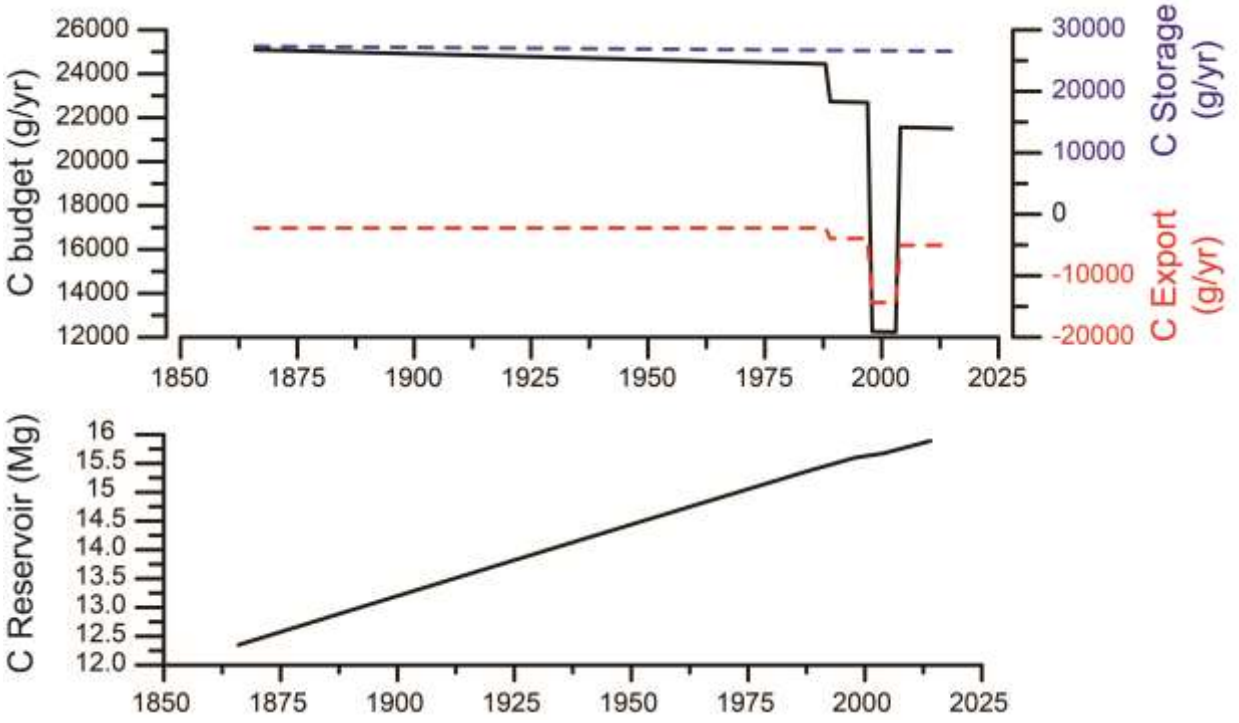

(Top) Carbon storage is denoted by the dashed blue line and carbon export is denoted by the dashed red line. The net budget is depicted by the solid black line. Note on the right y-axis the difference in limits for carbon storage and export. (Bottom) The carbon reservoir from 1866 to 2014.

Figure 3.9. Onslow Beach F1 and F2 carbon budgets and reservoirs

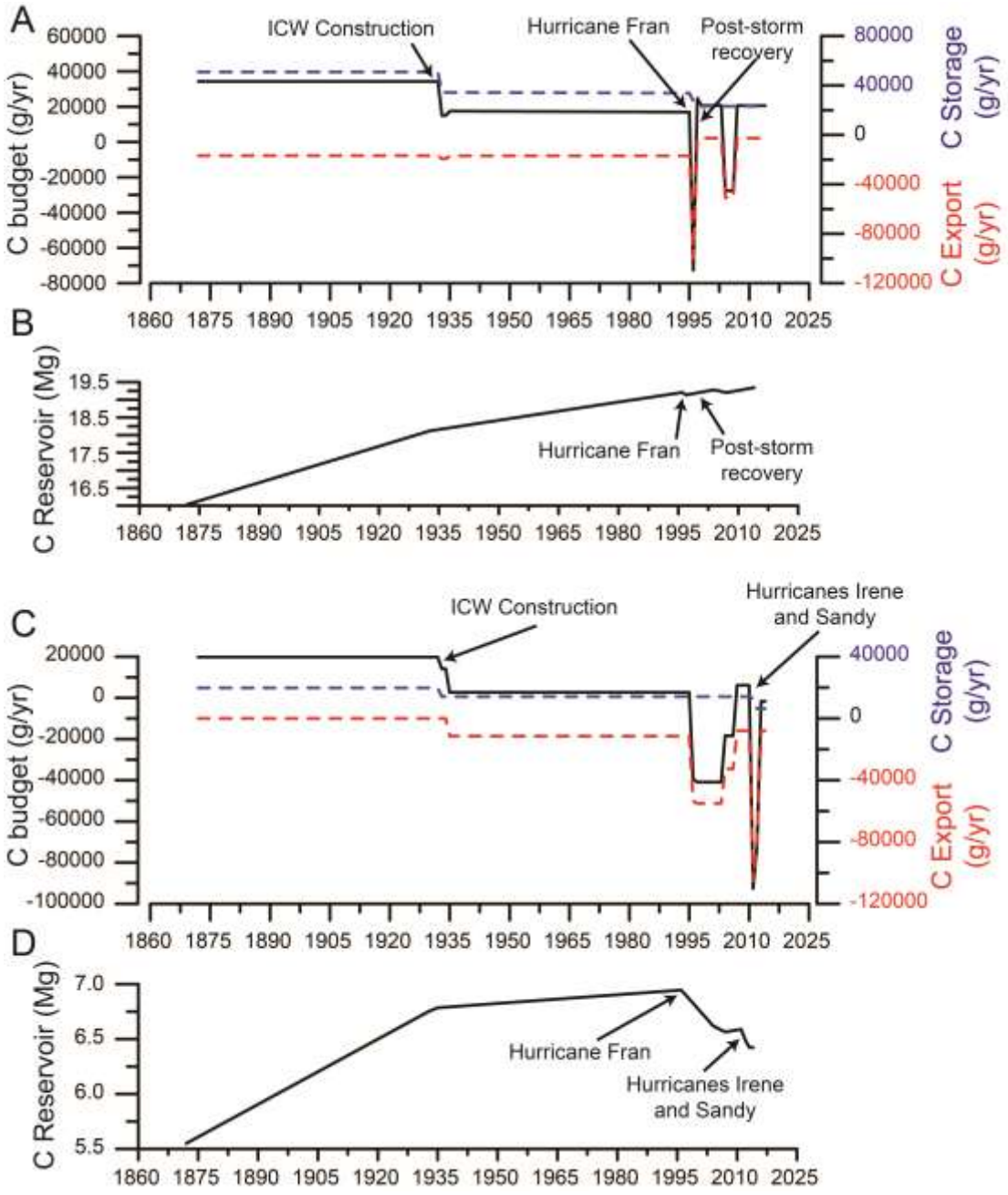

F1 and F2 carbon budgets through time are shown in panels A and C, respectively. Carbon storage is depicted in these panels as a dashed blue line, carbon export as a dashed red line, and net carbon budget as a solid black line. Note the difference in limits for carbon export and storage on the second y-axis in panels A and C. F1 and F2 carbon reservoirs through time are shown in panels B and D, respectively. The timing of the ICW dredging and storm impacts are annotated on each graph.

decreases in marsh area from dredging of the ICW and burial by washover control the variability in carbon storage at Onslow Beach (Figure 3.9). Carbon storage progressively decreases through time in response to marsh erosion and overwash (Figure 3.9). Variability in oceanfront erosion rates drive variations in carbon export because rates of backbarrier marsh erosion do not change at both sites. The shoreface carbon inventories at F1 and F2 are assumed to be constant through time and were measured as 13,394 ± 22.8 g C m^{-2} (core F1-2) and 10,388.18 ± 17.7 g C m^{-2} (core F2-1), respectively. Carbon export rates are highest during storms when erosion rates are highest (Figure 3.9). For example, high export rates in 1996 at F1 and F2 are associated with Hurricane Fran and high export rates in 2011 were associated with Hurricane Irene at F2. During storm recovery phases, such as at F1 following Hurricane Fran, or other instances in time when the barrier shoreface is not eroding there is no carbon export (Figure 3.9).

At the Onslow Beach sites, the carbon budget varied considerably over the past century, but both remained carbon sinks until the 1990s (Figure 3.9). The net budget decreased more rapidly at F2 because of high oceanfront shoreline erosion rates and a large loss of carbon storage capacity from excavation and burial of marsh during ICW construction in 1932. Throughout this time, however, the carbon reservoir progressively increased at both sites. Both sites became a carbon source in 1996 during Hurricane Fran, which resulted in the loss of some of the carbon reservoir. At F1, the transition to a carbon source during Hurricane Fran resulted from both high erosion and washover deposition that reduced backbarrier marsh carbon storage, while at F2 the transition was the result of high shoreface erosion rates. F1 transitioned back and forth between a carbon sink and source after the storm because the beach fluctuated between accreting and eroding. A similar pattern was observed at F2; however, the site only temporarily transitioned back to a carbon sink after Hurricane Fran because erosion persisted (Figure 3.9).

Hurricanes Irene and Sandy resulted in a further decrease in the carbon budget at F2 in response to high erosion rates and burial of backbarrier marsh by washover deposition. F2 remains a source of carbon because of diminished backbarrier marsh area and sustained carbon export from shoreface erosion and the carbon reservoir at F2 has generally been declining since 1996.

3.4. Discussion

The impact of erosion and overwash on the barrier island carbon budget varies depending on the evolutionary stage of a barrier island. Great Island represents an example of an early stage transgressive barrier and the wide backbarrier lagoon behind the island allowed for the formation of a large flood-tidal delta that was eventually colonized by saltmarsh. This expansive marsh stores a large amount of carbon annually, which buffers the impact of carbon export from erosion as well as any lost storage capacity from overwash deposition. Over the past century, Great Island has been above the threshold width where erosion and overwash substantially impact the annual carbon budget, thus even though carbon is exported from shoreface erosion, the carbon reservoir has been increasing because storage in the extensive marsh exceeds export.

Given the wide backbarrier lagoon and its geologic history (Heron et al., 1984), Great Island is likely to continue to go through cycles of narrowing and widening over centuries to millennia until it reaches the mainland. During narrowing phases, carbon export will occur from persistent shoreface and backbarrier erosion, which will cause narrowing of the backbarrier marsh. The carbon reservoir will continue to increase during this phase until the marsh has narrowed to a point where carbon export outpaces storage. At this point, the reservoir will begin to decrease as the island functions as a carbon source. Once the barrier island reaches a critical width an inlet breach will occur (Leatherman, 1979, 1983; Timmons et al., 2010) resulting in a rapid increase in the carbon reservoir and resetting the system.

As the barrier approaches the mainland and enters the middle stages of transgression, the backbarrier lagoon is filled in and inlet formation will not occur, thus new marsh formation can only occur in association with washover deposits. With sustained transgression, the backbarrier marsh of a middle-stage barrier island will continue to narrow through time; however, carbon storage is still likely outpacing carbon export during non-storm periods. During storm events a site may temporarily transition to a carbon source in response to increased carbon export through shoreface erosion and/or a decrease in carbon storage through washover burial. The carbon reservoir stored within the barrier will decrease during these events; however, the site should transition back to a sink if increased rates of erosion are not sustained after the event. Onslow Beach Site F1 exemplifies a barrier in the middle stages of transgression. This site has a wide backbarrier marsh and generally functioned as a carbon sink over the last century. Hurricane Fran, which resulted in high erosion rates and overwash deposition, temporarily transitioned the site to a carbon source and decreased the carbon reservoir slightly; however, the site returned to functioning as a carbon sink during post-storm recovery.

As the barrier island continues to narrow it enters the late stages of transgression, where the barrier is close to the mainland and the backbarrier marsh is narrow. At this point, erosion and overwash have a large negative impact on the carbon budget because carbon storage in the narrow backbarrier marsh is relatively low. Carbon export is likely always outpacing carbon storage not just during storm events; however, storm erosion can result in even greater carbon export and overwash can further reduce carbon storage. During the late stages of transgression the island is likely functioning as a sustained carbon source and the carbon reservoir is continuously decreasing.

Onslow Beach Site F2 likely just reached or is very close to entering the late stages of transgression. The backbarrier marsh is very narrow and erosion and overwash during the late 20th century and early 21st century resulted in the island primarily functioning as a carbon source, which reduced the carbon reservoir. The large washover deposit that formed at F2 in response to Irene and Sandy could eventually be recolonized by saltmarsh, which would increase the area for carbon storage and transition the site back to a carbon sink. Given that the fan is currently supratidal, sea-level would need to reach the elevation of the fan before intertidal saltmarsh formation will occur.

Storms appear to be the primary drivers of rapid transitions from a barrier island site functioning as a carbon sink to carbon source because they induce large amounts of carbon export at the beach via erosion and reduce backbarrier marsh carbon storage through overwash burial. The impact of storms on the carbon budget was greatest at the middle and late stage transgressive barrier sites at Onslow Beach. An increase in storminess will likely have a dramatic effect on the carbon budget of middle and late-stage transgressive barriers because an increase in erosion and overwash will hasten the islands transition to a sustained carbon source. Although an increase in storminess could increase carbon export at early stage transgressive barriers like Great Island, high amounts of carbon storage across the wide backbarrier marshes should buffer these impacts. More intense storms will likely result in the formation of more inlets and flood-tidal deltas (Mallinson et al., 2011), which could alter the rate at which the cycles of barrier narrowing and widening occur at early stage barrier islands. An increase in storminess may also result in an increase in the rate of barrier island transgression, thus early stage sites may transition more rapidly to middle stage barriers, or middle or late stage barriers may narrow more rapidly.

In addition to changes in marsh area due to backbarrier shoreline erosion and overwash, rates of carbon input to the carbon reservoir can increase or decrease with changes in the rate of sea-level rise (Kirwan and Mudd, 2012). Increased rates of sea-level rise could increase carbon storage by increasing accommodation space for marsh accretion (Morris et al., 2002; Morris et al., 2012), but will also increase the rate of barrier island rollover (Fitzgerald et al., 2008; Lorenzo-Trueba and Ashton, 2014), potentially leading to enhanced carbon export. Similar to the impacts from an increase in storminess, accelerated sea-level rise will have a greater impact on middle and late stage barrier islands than early stage barriers. Rapid barrier rollover will increase the rate of carbon export and will further reduce the area of backbarrier marsh for carbon storage through washover, potentially overwhelming the increased rate of vertical marsh accretion induced by sea-level rise. Overwash could create new marsh substrate at these sites (Godfrey and Godfrey, 1974); however, the washover deposit must be at an intertidal elevation to support marsh colonization and that landscape setting often decreases in area once a barrier island approaches the mainland. In locations where a barrier island is approaching steep mainland gradients, such as Onslow Beach, or coastal infrastructure it is unlikely that backbarrier marsh will be able to expand landward once the island reaches the mainland, thus the carbon reservoir could not be sustained.

3.5. Conclusions

Transgressive barrier islands are highly dynamic environments that have the capacity to store large amounts of carbon in marsh deposits; however, results from this study suggest that transgressive processes must be included in carbon budget assessments. Barrier island transgression can increase the carbon reservoir within a barrier by creating new marsh substrate via overwash and flood tidal delta deposition, but will also export carbon through shoreface and

backbarrier erosion. Prior to this study, the processes associated with barrier island rollover had not been considered in the carbon literature; however our field data and modelling results suggest that the barrier island carbon budget is sensitive to changes in the ocean shoreline erosion rate as well as marsh area. Global wetland inventories consider only backbarrier marsh area in projections of carbon storage and thus are ignoring the processes associated with barrier island response to storms, sea-level rise and anthropogenic disturbances. The sustainability of a barrier island as a carbon sink as well as the degree to which storms and human activities impact the carbon budget appears to be tied to a barriers evolutionary stage. Barrier islands in the early stages of transgression will likely remain carbon sinks for centuries because backbarrier accommodation space is conducive for new marsh to continue to form via inlet formation and overwash processes. In contrast, barrier islands that are in the middle stage of transgression will primarily function as carbon sinks, but will transition to sources during storms when erosion rates increase and overwash deposition occurs. As a barrier island transitions to the late stage of transgression it will primarily function as a carbon source as the marsh is narrow and export rates likely continuously exceed storage rates. However, if export rates slow or stop, allowing carbon storage to exceed export, even a barrier island in the late stages of transgression can transition back to functioning as a carbon sink. In order to manage a barrier island with respect to both the present and future status of carbon storage, the natural processes associated with transgression, such as erosion and overwash, must be considered.

APPENDIX 1.1: AVERAGE BEACH GRADIENT (SOLID DARK LINE) AND WIDTH (DASHED GRAY LINE) ±1 SD FOR EACH FOCUS SITE AT ONSLOW BEACH

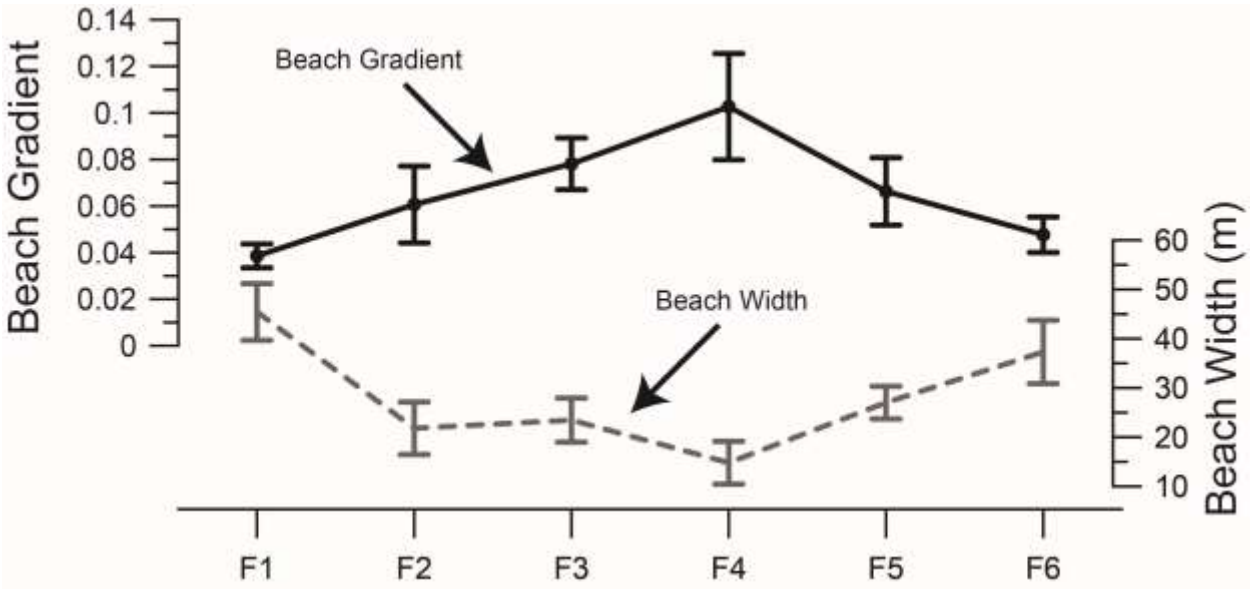

APPENDIX 1.2: MODELS USED TO FILL IN WAVE DATA GAPS

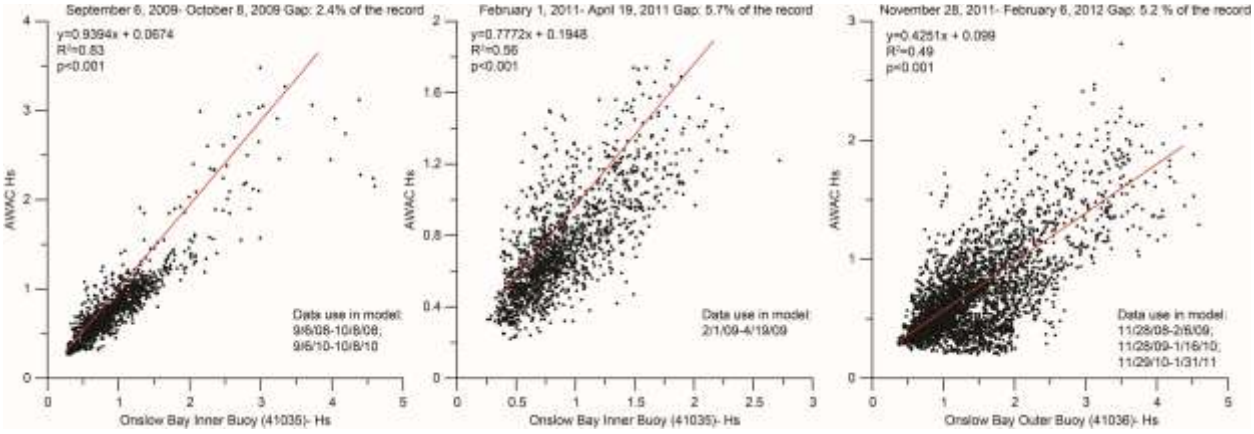

APPENDIX 2.1. RADIOCARBON DATES FOR CARROT ISLAND SAMPLES

Lab ID	Core location	Core name	Sample depth (cm)	Material dated	Conventional ^{14}C age: yr BP	Calib. ^{14}C age: cal BP; 2σ	Calib. ^{14}C age: cal AD; 2σ	Dep. Env.
Beta-345368	Ramped	CIR-12-2	71-73	Plant	500 +/- 30 BP	540-510	1400-1440	Base of marsh
Beta-345369	Scarped	CIS-12-21	42-46	Plant	420 +/- 30 BP	520-460	1430-1490	Base of marsh
Beta-344129	Scarped	CIS-12-19	260	*Chioni cancellata*	1630 +/- 30 BP	1250-910	700-1040	Lagoon

APPENDIX 3.1. RADIOCARBON DATES FROM ONSLOW BEACH AND CORE BANKS. ALL SAMPLES WERE ANALYZED BY BETA ANALYTIC. THE AGE WITH THE MOST RELATIVE AREA UNDER THE PROBABILITY DISTRIBUTION WAS USED AS THE MOST LIKELY MARSH AGE. IN SAMPLES WHERE THERE WAS A SIMILAR PROBABILITY FOR MULTIPLE RANGES, THE ENTIRE RANGE WAS USED TO ESTIMATE THE AGE (E.G. OB-F1-M3).

Sample Name	Sample depth-from top of core (cm)	Conventional C14 age: cal AD	Calibrated C14 age: cal AD; 2 sigma	Relative area under probability distribution	Age cal BP	Age error cal BP
OB-F1-2	55-57	Modern			0	
OB-F1-2	84-87	250 ± 40	1514- 1600 1617- 1683 1735- 1805 1933- 1950*	0.257 0.445 0.247 0.051	300	33
OB-F1-6	50-52	145 ± 25	1669- 1708 1718- 1781 1798- 1827 1831- 1888 1911- 1946	0.168 0.32 0.121 0.212 0.178	200	32
OB-F1-M3	33-35	350 ± 25	1460- 1529 1541- 1635	0.435 0.565	402	88
OB-F1-M2	65-68	730 ± 30	1224- 1237 1241- 1297	0.033 0.967	681	28
OB-F1-M4	63-65	675 ± 25	1275- 1313 1357- 1388	0.62 0.38	656	19
OB-F1-M1	46-48	145 ± 35	1668- 1782 1797- 1891 1908- 1949	0.471 0.36 0.169	225	57
OB-F2-1	110-113	450 ± 30	1415- 1478	1	504	32
OB-F2-2	55-60	140 ± 30	1669- 1780 1798- 1891 1909- 1944	0.454 0.383 0.163	170	111
OB-F2-2	96-99	205 ± 25	1649- 1682	0.298	180	35

			1736- 1805 1935- 1950*	0.559 0.142		
OB-F2-2	110- 112	215 ± 25	1646- 1681 1738- 1755 1762- 1803 1937- 1950*	0.38 0.047 0.454 0.118	226	79
OB-F2-5	82-85	Modern			0	
OB-F2-7	39-41	255 ± 25	1524- 1558 1631- 1669 1780- 1798 1944- 1950*	0.132 0.703 0.153 0.011	300	19
OB-F2-M3	38-40	205 ± 40	1640- 1697 1724- 1815 1834- 1878 1916- 1950*	0.288 0.516 0.041 0.155	180	46
OB-F2-M2	29-31	130 ± 25	1677- 1766 1772- 1776 1800- 1893 1906- 1940	0.37 0.008 0.464 0.158	165	108
OB-F2-M1	38-40	110 ± 30	1681- 1739 1750- 1762 1802- 1938	0.286 0.02 0.694	80	68
CB-9	35-40	420 ± 30	1513-1600 1616-1666	0.566 0.403	359	77

REFERENCES

Allan, J. C., and P. D. Komar (2006), Climate controls on US West Coast erosion processes, *J. Coastal Res.*, 22(3), 511-529, doi: 10.2112/03-0108.1.

Barbier, E.B., Hacker, S.D., Kennedy, C., Koch, E.W., Stier, A.C., Silliman, B.R., 2011. The value of estuarine and coastal ecosystem services. Ecol. Monogr. 81, 169–193. doi:10.1890/10-1510.1

Bauer, J.E., Cai, W.-J., Raymond, P. a, Bianchi, T.S., Hopkinson, C.S., Regnier, P. a G., 2013. The changing carbon cycle of the coastal ocean. Nature 504, 61–70. doi:10.1038/nature12857

Benton, S.B., C.J. Bellis, J.M. Knisel, M.F. Overton, and J.S. Fisher (2004), Long-term Average Annual Erosion Rate Update: Methods Report (March 18), *NC Division of Coastal Management, NC Coastal Resources Commission*, 23.

Berelson, W., Heron, S., 1985. Correlations between Holocene flood tidal delta and barrier island inlet fill sequences: Back Sound-Shackleford Banks, North Carolina. Sedimentology 32, 215–222.

Blaha, J. P. (1984), Fluctuations of monthly sea level as related to the intensity of the Gulf Stream from Key West to Norfolk, *J. of Geophys. Res.*, 89(C5), 8033-8042, doi: 10.1029/JC089iC05p08033.

Bridgham, S., Megonigal, J., Keller, J., 2006. The carbon balance of North American wetlands. Wetlands 26, 889–916.

Cahoon, D.R., Day Jr., J.W., Reed, D.J., Young, R.S., 1998. Chapter 3 : Global Climate Change and Sea-level Rise : Estimating the Potential for Submergence of Coastal Wetlands Vertical Buildup of the Marsh Surface. Biological Science Report. USGS/BRD/BSR-1998-0002

Cai, W.-J., 2011. Estuarine and coastal ocean carbon paradox: CO2 sinks or sites of terrestrial carbon incineration? Ann. Rev. Mar. Sci. 3, 123–45. doi:10.1146/annurev-marine-120709-142723

Chmura, G.L., 2013. What do we need to assess the sustainability of the tidal saltmarsh carbon sink? Ocean Coast. Manag. 83, 25–31. doi:10.1016/j.ocecoaman.2011.09.006

Chmura, G.L., Anisfeld, S.C., Cahoon, D.R., Lynch, J.C., 2003. Global carbon sequestration in tidal, saline wetland soils. Global Biogeochem. Cycles 17. doi:10.1029/2002GB001917

Choi, Y., Wang, Y., 2004. Dynamics of carbon sequestration in a coastal wetland using radiocarbon measurements. Global Biogeochem. Cycles 18. doi:10.1029/2004GB002261

Coverdale, T.C., Brisson, C.P., Young, E.W., Yin, S.F., Donnelly, J.P., Bertness, M.D., 2014. Indirect human impacts reverse centuries of carbon sequestration and saltmarsh accretion. PLoS One 9, e93296. doi:10.1371/journal.pone.0093296

Connor, R.F., Chmura, G.L., Beecher, C.B., 2001. Carbon accumulation in Bay of Fundy salt marshes: implications for restoration of reclaimed marshes. Glob. Biogeochem. … 15, 943–954.

Crooks, S., Herr, D., Laffoley, D., Tamelander, J., Vandever, J., 2011. Regulating Climate Change Through Restoration and Management of Coastal Wetlands and Near-shore Marine Ecosystems: Mitigation Potential and Policy Opportunities. Washington, Gland, San Francisco.

Culver, S. J., C. G. Pre, D. J. Mallinson, S. R. Riggs, D. R. Corbett, J. Foley, M. Hale, L. Metger, J. Ricardo, and J. Rosenberger (2007), Late Holocene barrier island collapse: Outer Banks, North Carolina, USA, *The Sedimentary Record*, 5(4), 4-8.

Davis, J.L., Currin, C. a, O'Brien, C., Raffenburg, C., Davis, A., 2015. Living Shorelines: Coastal Resilience with a Blue Carbon Benefit. PLoS One 10, e0142595. doi:10.1371/journal.pone.0142595

Day, J., Britsch, L., Hawes, S., Shaffer, G., 2000. Pattern and process of land loss in the Mississippi Delta: a spatial and temporal analysis of wetland habitat change. Estuaries 23, 425–438.

D'Alpaos, A., Lanzoni, S., Marani, M., Rinaldo, A., 2007. Landscape evolution in tidal embayments: Modeling the interplay of erosion, sedimentation, and vegetation dynamics. J. Geophys. Res. 112, F01008. doi:10.1029/2006JF000537

De Groot, A., Veeneklaas, R., Bakker, J., 2011. Sand in the salt marsh: Contribution of high-energy conditions to salt-marsh accretion. Mar. Geol. 282, 240–254. doi:10.1016/j.margeo.2011.03.002

Dingler, J. R., and T. E. Reiss (2002), Changes to Monterey Bay beaches from the end of the 1982–83 El Niño through the 1997–98 El Niño, *Mar. Geol.*, 181(1), 249-263, doi: 10.1016/S0025-3227(01)00270-5.

Doody, J., 2004. "Coastal squeeze"—an historical perspective. J. Coast. Conserv. 10, 129–138.

Doody, J.P., 2013. Coastal squeeze and managed realignment in southeast England, does it tell us anything about the future? Ocean Coast. Manag. 79, 34–41. doi:10.1016/j.ocecoaman.2012.05.008

Donnelly, C., Kraus, N., Larson, M., 2006. State of Knowledge on Measurement and Modeling of Coastal Overwash. J. Coast. Res. 224, 965–991. doi:10.2112/04-0431.1

Duarte, C., Middelburg, J., Caraco, N., 2005. Major role of marine vegetation on the oceanic carbon cycle. Biogeosciences 1, 1–8.

Duarte, C.M., 2009. Global Loss of Coastal Habitats: Rates, Causes, and Consequences. Madrid.

Duarte, C.M., Dennison, W.C., Orth, R.J.W., Carruthers, T.J.B., 2008. The Charisma of Coastal Ecosystems: Addressing the Imbalance. Estuaries and Coasts 31, 233–238. doi:10.1007/s12237-008-9038-7

Eichler, T., and W. Higgins (2006), Climatology and ENSO-related variability of North American extratropical cyclone activity, *J. of Climate*, 19(10), 2076-2093, doi: 10.1175/JCLI3725.1.

Elliott, E.A., McKee, B.A., Rodriguez, A.B., 2015. The utility of estuarine settling basins for constructing multi-decadal, high-resolution records of sedimentation. Estuar. Coast. Shelf Sci. 164, 105–114. doi:10.1016/j.ecss.2015.06.002

Ember, L., Williams, D., Morris, J., 1987. Processes that influence carbon isotope variations in salt marsh sediments. Mar. Ecol. Prog. Ser. 36, 33–42.

Ezer, T. (2001), Can long-term variability in the Gulf Stream transport be inferred from sea level? *Geophys. Res. Lett.*, 28(6), 1031-1034, doi: 10.1029/2000GL011640.

Ezer, T. (2013), Sea level rise, spatially uneven and temporally unsteady: Why the U.S. East Coast, the global tide gauge record, and the global altimeter data show different trends, *Geophys. Res. Lett.*, 40, 5439-5444, doi:10.1002/2013GL057952.

Ezer, T., L. P. Atkinson, W. B. Corlett, and J. L. Blanco (2013), Gulf Stream's induced sea level rise and variability along the US mid-Atlantic coast, *J. of Geophys. Research: Oceans*, 118(2), 685-697, doi: 10.1002/jgrc.20091.

Fagherazzi, S., Kirwan, M., 2012. Numerical models of saltmarsh evolution: ecological, geomorphic, and climatic factors. Rev. 1–28. doi:10.1029/2011RG000359.1

FitzGerald, D.M., 2008. Coastal Impacts Due to Sea-Level Rise. Annu. Rev. Earth Planet. Sci. 36, 601–647. doi:10.1146/annurev.earth.35.031306.140139

Gebrehiwet, T., Koretsky, C.M., Krishnamurthy, R.V., 2008. Influence of Spartina and Juncus on saltmarsh sediments. III. Organic geochemistry. Chem. Geol. 255, 114–119. doi:10.1016/j.chemgeo.2008.06.015

Gedan, K.B., Silliman, B.R., Bertness, M.D., 2009. Centuries of human-driven change in saltmarsh ecosystems. Ann. Rev. Mar. Sci. 1, 117–41. doi:10.1146/annurev.marine.010908.163930

Godfrey, P.J., Godfrey, M.M., 1974. The role of overwash and inlet dynamics in the formation of salt marshes on North Carolina barrier islands, ECOLOGY OF HALOPHYTES. Academic Press, New York. doi:10.1016/B978-0-12-586450-3.50016-0

Heron, S., Moslow, T., Berelson, W., 1984. Holocene sedimentation of a wave-dominated barrier island shoreline: Cape Lookout, North Carolina. Mar. Geol. 60, 413–434.

Holman, R.A. (1986), Extreme value statistics for wave run-up on a natural beach, *Coastal Eng.*, 9, 527-544, doi:10.1016/0378-3839(86)90002-5.

Hong, B., W. Sturges, and A. J. Clarke (2000), Sea level on the US east coast: Decadal variability caused by open ocean wind-curl forcing, *J. of Phys. Oceanogr.*, 30(8), 2088-2098, doi: 10.1175/1520-0485(2000)030<2088:SLOTUS>2.0.CO;2.

Houghton, R. A., 2007. Balancing the Global Carbon Budget. Annu. Rev. Earth Planet. Sci. 35, 313–347. doi:10.1146/annurev.earth.35.031306.140057

Houser, C., 2010. Relative Importance of Vessel-Generated and Wind Waves to Saltmarsh Erosion in a Restricted Fetch Environment. J. Coast. Res. 262, 230–240. doi:10.2112/08-1084.1

Intergovernmental Panel on Climate Change. Climate Change 2014–Impacts, Adaptation and Vulnerability: Regional Aspects. Cambridge University Press, 2014.

Keim, B.D., R.A. Muller, and G.W. Stone (2004), Spatial and temporal variability of coastal storms in the North Atlantic Basin, *Mar. Geol.*, 210(1-4), 7-15, doi: 10.1016/j.margeo.2003.12.006.

Kirwan, M.L., Guntenspergen, G.R., D'Alpaos, A., Morris, J.T., Mudd, S.M., Temmerman, S., 2010. Limits on the adaptability of coastal marshes to rising sea level. Geophys. Res. Lett. 37. doi:10.1029/2010GL045489

Kirwan, M.L., Megonigal, J.P., 2013. Tidal wetland stability in the face of human impacts and sea-level rise. Nature 504, 53–60. doi:10.1038/nature12856

Kirwan, M.L., Mudd, S.M., 2012. Response of salt-marsh carbon accumulation to climate change. Nature 489, 550–3. doi:10.1038/nature11440

Kolker, A. S., and S. Hameed (2007), Meteorologically driven trends in sea level rise, *Geophys. Res. Lett.*, 34(23), doi: 10.1029/2007GL031814.

Kulawardhana, R.W., Feagin, R. A., Popescu, S.C., Boutton, T.W., Yeager, K.M., Bianchi, T.S., 2015. The role of elevation, relative sea-level history and vegetation transition in determining carbon distribution in Spartina alterniflora dominated salt marshes. Estuar. Coast. Shelf Sci. 154, 48–57. doi:10.1016/j.ecss.2014.12.032

Leatherman, S.P., 1979. Migration of Assateague Island, Maryland, by inlet and overwash processes. Geology 7, 104–107. doi:10.1130/0091-7613(1979)7

Leatherman, S.P., 1983. Barrier dynamics and landward migration with Holocene sea-level rise. Nature 301, 415–417.

Leonard, L., Luther, M., 1995. Flow hydrodynamics in tidal marsh canopies. Limnol. Oceanogr. 40, 1474–1484.

Leonardi, N., Fagherazzi, S., 2014. How waves shape saltmarshes. Geology 42, 887–890. doi:10.1130/G35751.1

Lorenzo-Trueba, J., Ashton, A.D., 2014. Rollover, drowning, and discontinuous retreat: Distinct modes of barrier response to sea-level rise arising from a simple morphodynamic model. J. Geophys. Res. Earth Surf. 119, 779–801. doi:10.1002/2013JF002941.

Mallinson, D., Culver, S., Riggs, S., Walsh, J., Ames, D., Smith, C., 2008. Past, present and future inlets of the Outer Banks barrier islands, North Carolina, East Carolina University …. Greenville, NC.

Mallinson, D.J., Smith, C.W., Mahan, S., Culver, S.J., McDowell, K., 2011. Barrier island response to late Holocene climate events, North Carolina, USA. Quat. Res. 76, 46–57. doi:10.1016/j.yqres.2011.05.001

Marani, M., D'Alpaos, a., Lanzoni, S., Santalucia, M., 2011. Understanding and predicting wave erosion of marsh edges. Geophys. Res. Lett. 38. doi:10.1029/2011GL048995

Mariotti, G., Fagherazzi, S., 2010. A numerical model for the coupled long-term evolution of saltmarshes and tidal flats. J. Geophys. Res. 115, F01004. doi:10.1029/2009JF001326

Mariotti, G., Fagherazzi, S., Wiberg, P.L., McGlathery, K.J., Carniello, L., Defina, a., 2010. Influence of storm surges and sea level on shallow tidal basin erosive processes. J. Geophys. Res. 115, C11012. doi:10.1029/2009JC005892

Mariotti, G., Fagherazzi, S., 2013. Critical width of tidal flats triggers marsh collapse in the absence of sea-level rise. Proc. Natl. Acad. Sci. U. S. A. 110, 5353–6. doi:10.1073/pnas.1219600110

Mattheus, C.R., Rodriguez, A.B., McKee, B.A., Currin, C.A., 2010. Impact of land-use change and hard structures on the evolution of fringing marsh shorelines. Estuar. Coast. Shelf Sci. 88, 365–376. doi:http://dx.doi.org/10.1016/j.ecss.2010.04.016

McCallum, B. E., J. A. Painter, and E. R. Frantz (2012), Monitoring Inland Storm Tide and Flooding from Hurricane Irene along the Atlantic Coast of the United States, August 2011, *US Geol. Surv. Open-File Report*, 1022

Mcleod, E., Chmura, G.L., Bouillon, S., Salm, R., Björk, M., Duarte, C.M., Lovelock, C.E., Schlesinger, W.H., Silliman, B.R., 2011. A blueprint for blue carbon: toward an improved understanding of the role of vegetated coastal habitats in sequestering CO2. Front. Ecol. Environ. 9, 552–560.

McLoughlin, S.M., Wiberg, P.L., Safak, I., McGlathery, K.J., 2014. Rates and Forcing of Marsh Edge Erosion in a Shallow Coastal Bay. Estuaries and Coasts 38, 620–638. doi:10.1007/s12237-014-9841-2

Middelburg, J., Nieuwenhuize, J., 1997. Organic carbon isotope systematics of coastal marshes. Estuar. Coast. Shelf Sci. 681–687.

Möller, I., Kudella, M., Rupprecht, F., 2014. Wave attenuation over coastal saltmarshes under storm surge conditions. Nat. 7, 727–731. doi:10.1038/NGEO2251

Moore, L., 2000. Shoreline mapping techniques. J. Coast. Res. 16, 111–124.

Morris, J. T., B. Kjerfve, and J. M. Dean (1990), Dependence of estuarine productivity on anomalies in mean sea level, *Limnology and Oceanography*, 35(4), 926-930.

Morris, J., Sundareshwar, P., Nietch, C., 2002. Responses of coastal wetlands to rising sea level. Ecology 83, 2869–2877.

Morris, J.T., Edwards, J., Crooks, S., Reyes, E., 2012. Assessment of Carbon Sequestration Potential in Coastal Wetlands, in: Lal, R., Lorenz, K., Hüttl, R.F., Schneider, B.U., von Braun, J. (Eds.), Recarbonization of the Biosphere. Springer Netherlands, Dordrecht, pp. 517–531. doi:10.1007/978-94-007-4159-1

Moslow, T., Heron, SD, J., 1978. Relict inlets: preservation and occurrence in the Holocene stratigraphy of southern Core Banks, North Carolina. J. Sedimentology, 8, 1275–1286.

Mudd, S.M., Howell, S.M., Morris, J.T., 2009. Impact of dynamic feedbacks between sedimentation, sea-level rise, and biomass production on near-surface marsh stratigraphy and carbon accumulation. Estuar. Coast. Shelf Sci. 82, 377–389. doi:10.1016/j.ecss.2009.01.028

Murray, B.C., Pendleton, L., Jenkins, W.A., Sifleet, S., 2011. Green Payments for Blue Carbon Economic Incentives for Protecting Threatened Coastal Habitats. Durham.

Needles, L.A., Lester, S.E., Ambrose, R., Andren, A., Beyeler, M., Connor, M.S., Eckman, J.E., Costa-Pierce, B. a., Gaines, S.D., Lafferty, K.D., Lenihan, H.S., Parrish, J., Peterson, M.S., Scaroni, A.E., Weis, J.S., Wendt, D.E., 2013. Managing Bay and Estuarine Ecosystems for Multiple Services. Estuaries and Coasts 38, 35–48. doi:10.1007/s12237-013-9602-7

Nellemann, C., Corcoran, F., Duarte, C.M., Valdes, L., DeYoung, C., Fonseca, L., Grimsditch, G., 2009. Blue Carbon: The Role of Healthy Oceans in Binding Carbon : a Rapid Response Assessment. UNEP/Earthprint.

Nicholls, R., Hoozemans, F., Marchand, M., 1999. Increasing flood risk and wetland losses due to global sea-level rise: regional and global analyses. Glob. Environ. Chang. 9.

Nyman, J. A., Walters, R.J., Delaune, R.D., Patrick, W.H., 2006. Marsh vertical accretion via vegetative growth. Estuar. Coast. Shelf Sci. 69, 370–380. doi:10.1016/j.ecss.2006.05.041

Ouyang, X., Lee, S.Y., 2014. Updated estimates of carbon accumulation rates in coastal marsh sediments. Biogeosciences 11, 5057–5071. doi:10.5194/bg-11-5057-2014

Pendleton, L., Donato, D.C., Murray, B.C., Crooks, S., Jenkins, W.A., Sifleet, S., Craft, C., Fourqurean, J.W., Kauffman, J.B., Marbà, N., Megonigal, P., Pidgeon, E., Herr, D., Gordon, D., Baldera, A., 2012. Estimating global "blue carbon" emissions from conversion and degradation of vegetated coastal ecosystems. PLoS One 7, e43542. doi:10.1371/journal.pone.0043542

Peterson, G., Turner, R., 1994. The value of saltmarsh edge vs interior as a habitat for fish and decapod crustaceans in a Louisiana tidal marsh. Estuaries 17, 235–262.

Pontee, N., 2013. Defining coastal squeeze: A discussion. Ocean Coast. Manag. 84, 204–207. doi:10.1016/j.ocecoaman.2013.07.010

Redfield, A.C., Rubin, M., 1962. The age of salt marsh peat and its relation to recent changes in sea level at Barnstable, Massachussetts. Proc. Natl. Acad. Sci. 48, 1728–1735.

Reed, D., 1988. Sediment dynamics and deposition in a retreating coastal salt marsh. Estuar. Coast. Shelf Sci. 26, 67–79.

Reed, D., 1995. The response of coastal marshes to sea-level rise: Survival or submergence? Earth Surf. Process. Landforms 20, 39–48. doi:10.1002/esp.3290200105

Reimer, P.J., Baillie, M.G.L., Bard, E., Bayliss, A., Beck, J.W., Blackwell, P.G., Bronk Ramsey, C., Buck, C.E., Burr, G.S., Edwards, R.L., Friedrich, M., Grootes, P.M., Guilderson, T.P., Hajdas, I., Heaton, T.J., Hogg, A.G., Hughen, K.A., Kaiser, K.F., Kromer, B., McCormac, F.G., Manning, S.W., Reimer, R.W., Richards, D.A., Southon, J.R., Talamo, S., Turney, C.S.M., van der Plicht, J., Weyhenmeyer, C.E., 2009. IntCal09 and Marine09 radiocarbon age calibration curves, 0-50,000 yeats cal BP. Radiocarbon 51, 1111–1150.

Reimer, P.J., Bard, E., Bayliss, A., Beck, W.J., Blackwell, P.G., Bronk Ramsey, C., Buck, C.E., Cheng, H., Edwards, R.L., Friedrich, M., Grootes, P.M., Guilderson, T.P., Haflidason, H., Hajdas, I., Hatte, C., Heaton, T.J., Hoffmann, D.L., Hogg, A.G., Hughen, K.A., Kaiser, K.F., Kromer, B., Manning, S.W., Niu, M., Reimer, R.W., Richards, D.A., Scott, E.M., Southon, J.R., Staff, R.A., Turney, C.S.M., van der Plicht, J., 2013. IntCal13 and Marine13 radiocarbon age calibration curves 0–50,000 years cal BP. Radiocarbon 55, 1869–1887.

Riggs. S.R., W.J. Cleary, and S.W. Snyder (1995), Influence of inherited geologic framework on barrier shoreface morphology and dynamics, *Mar. Geol.*, 126(1-4), 213-234, doi: 10.1016/0025-3227(95)00079-E.

Roberts, H., 1997. Dynamic changes of the Holocene Mississippi River delta plain: the delta cycle. J. Coast. Res. 13, 605–627.

Robertson V, W., K. Zhang, and D. Whitman (2007), Hurricane-induced beach change derived from airborne laser measurements near Panama City, Florida, *Mar. Geol.*, 237(3), 191-205, doi: 10.1016/j.margeo.2006.11.003.

Rodriguez, A. B., and C. T. Meyer (2006), Sea-level variation during the Holocene deduced from the morphologic and stratigraphic evolution of Morgan Peninsula, Alabama, USA, *J. of Sed. Res.*, 76(2), 257-269, doi: 10.2110/jsr.2006.018.

Rodriguez, A. B., P. L. Rodriguez, and S. R. Fegley (2012), One-year along-beach variation in the maximum depth of erosion resulting from irregular shoreline morphology, *Mar. Geol.*, 291, 12-23, doi: 10.1016/j.margeo.2011.10.010.

Rodriguez, A. B., S. R. Fegley, J. T. Ridge, B. M. VanDusen, and N. Anderson (2013), Contribution of aeolian sand to backbarrier marsh sedimentation, *Estuarine, Coastal and Shelf Science*, 117(0), 248-259, doi: 10.1016/j.ecss.2012.12.001.

Rodriguez, A.B., Fodrie, F.J., Ridge, J.T., Lindquist, N.L., Theuerkauf, E.J., Coleman, S.E., Grabowski, J.H., Brodeur, M.C., Gittman, R.K., Keller, D.E., Kenworthy, M.D., 2014. Oyster reefs can outpace sea-level rise. Nat. Clim. C 1–5. doi:10.1038/NCLIMATE2216

Ruggiero, P., P. D. Komar, W. G. McDougal, J. J. Marra, and R. A. Beach (2001), Wave runup, extreme water levels and the erosion of properties backing beaches, *J. Coastal Res.*, 17(2), 407-419.

Sallenger, A. H., K. S. Doran, and P. Howd (2012), Hotspot of accelerated sea-level rise on the Atlantic coast of North America, *Nat. Clim. Change*, 2, 884-888, doi:10.1038/NCILMATE1597.

Schlesinger, W.H., 1997. Biogeochemistry: An Analysis of Global Change, 2nd ed. Academic Press, San Diego.

Schwimmer, R.A., 2001. Rates and Processes of Marsh Shoreline Erosion in Rehoboth Bay, Delaware, U.S.A. J. Coast. Res. 17, 672–683.

Sokal, R.R., and F.J. Rohlf (2012), Biometry, Fourth Edition, W.H. Freeman, San Francisco, CA., 937pp.,

Stockdon, H. F., A. H. Sallenger Jr, R. A. Holman, and P. A. Howd (2007), A simple model for the spatially-variable coastal response to hurricanes, *Mar. Geol.*, 238(1), 1-20, doi: 10.1016/j.margeo.2006.11.004.

Storlazzi, C.D., and G.B. Griggs (2000), Influence of El Nino-Southern Oscillation (ENSO) events on the evolution of central California's shoreline, *Geol. Soc. Of Am. Bull.*, 112(2), 236-249, doi: 10.1130/0016-7606(2000)112<236:IOENOE>2.0.CO;2.

Susman, K.R., Heron, S.D., 1979. Evolution of a barrier island, Shackleford Banks, Carteret County, North Carolina. Geol. Soc. Am. Bull. 90.

Sweet, W., C. Zervas, and S. Gill (2009), Elevated East Coast Sea Level Anomaly: June- July 2009, NOAA Technical Report NOS CO-OPS 051.

Sweet, W.V., and C. Zervas (2011), Cool-Season Sea Level Anomalies and Storm Surges along the US East Coast: Climatology and Comparison with the 2009/19 El Nino, *Monthly Weather Rev.*, 139(7), 2290-2299, doi: 10.1175/MWR-D-10-05043.1.

Temmerman, S., Govers, G., Wartel, S., Meire, P., 2003a. Spatial and temporal factors controlling short-term sedimentation in a salt and freshwater tidal marsh, Scheldt estuary, Belgium, SW Netherlands. Earth Surf. Process. Landforms 28, 739–755. doi:10.1002/esp.495

Temmerman, S., Govers, G., Meire, P., Wartel, S., 2003b. Modelling long-term tidal marsh growth under changing tidal conditions and suspended sediment concentrations, Scheldt estuary, Belgium. Mar. Geol. 193, 151–169. doi:10.1016/S0025-3227(02)00642-4

Temmerman, S., Govers, G., Wartel, S., Meire, P., 2004. Modelling estuarine variations in tidal marsh sedimentation: response to changing sea level and suspended sediment concentrations. Mar. Geol. 212, 1–19. doi:10.1016/j.margeo.2004.10.021

Theuerkauf, E. J., and A. B. Rodriguez (2012), Impacts of transect location and variations in along-beach morphology on measuring volume change, *J. Coastal Res.*, 28(3), 707-718, doi: 10.2112/JCOASTRES-D-11-00112.1.

Theuerkauf, E.J., Rodriguez, A.B., 2014. Evaluating proxies for estimating subaerial beach volume change across increasing time scales and various morphologies. Earth Surf. Process. Landforms 39, 593–604. doi:10.1002/esp.3467

Theuerkauf, E.J., Stephens, J.D., Ridge, J.T., Fodrie, F.J., Rodriguez, A.B., 2015. Carbon export from fringing saltmarsh shoreline erosion overwhelms carbon storage across a critical width threshold. Estuar. Coast. Shelf Sci. 164, 367–378. doi:10.1016/j.ecss.2015.08.001

Thieler ER, Himmelstoss EA, Zichichi JL, Ergul A. 2009, Digital Shoreline Analysis System (DSAS) version 4.0—An ArcGIS extension for calculating shoreline change: U.S. Geological Survey Open-File Report 2008-1278.

Timmons, E. A., A. B. Rodriguez, C. R. Mattheus, and R. DeWitt (2010), Transition of a regressive to a transgressive barrier island due to back-barrier erosion, increased storminess, and low sediment supply: Bogue Banks, North Carolina, USA, *Mar. Geol.*, 278(1), 100-114, doi: 10.1016/j.margeo.2010.09.006.

VanDusen, B., Theuerkauf, E., 2016. Monitoring overwash using water-level loggers resolves frequent inundation and run-up events. Geomorphology 254, 32–40. doi:10.1016/j.geomorph.2015.11.010

Van de Koppel, J., van der Wal, D., Bakker, J.P., Herman, P.M.J., 2005. Self-organization and vegetation collapse in saltmarsh ecosystems. Am. Nat. 165, E1–12. doi:10.1086/426602

Vespremeanu-Stroe, A., Ş. Constantinescu, F. Tătui, and L. Giosan (2007), Multi-decadal Evolution and North Atlantic Oscillation Influences on the Dynamics of the Danube Delta Shoreline, *J. Coastal Res.*, SI 50, 157-162, ISSN 0749.0208.

Weber, K. M., J. H. List, and K. L. Morgan (2005), An operational mean high water datum for determination of shoreline position from topographic lidar data, US Geological Survey.

Yu, W., 2012. Impacts of storms and sea-level rise on coastal evolution between two capes: Onslow Bay, North Carolina. Master's Thesis. The University of North Carolina at Chapel Hill.

Zehetner, F., 2010. Does organic carbon sequestration in volcanic soils offset volcanic CO2 emissions? Quat. Sci. Rev. 29, 1313–1316. doi:10.1016/j.quascirev.2010.03.003

Zervas, C. (2001), Sea Level Variations of the United States 1854-1999, NOAA Technical Report NOS CO-OPS 036.

Zhang, K., B. C. Douglas, and S. P. Leatherman (2004), Global warming and coastal erosion, *Climatic Change*, 64(1-2), 41-58, doi: 10.1023/B:CLIM.0000024690.32682.48.